

Research Paper

MRI and histological evaluation of pulsed focused ultrasound and microbubbles treatment effects in the brain

Zsafia I Kovacs¹✉, Tsang-Wei Tu^{1,2,3}, Maggie Sundby¹, Farhan Qureshi¹, Bobbi K Lewis¹, Neekita Jikaria¹, Scott R Burks¹, Joseph A Frank^{1,4}✉

1. Frank Laboratory, Radiology and Imaging Sciences, Clinical Center, National Institutes of Health, Bethesda
2. Center for Neuroscience and Regenerative Medicine, Uniformed Services University of the Health Sciences, Bethesda
3. Molecular Imaging Laboratory, Department of Radiology, Howard University, Washington DC
4. National Institute of Biomedical Imaging and Bioengineering, National Institutes of Health, Bethesda

✉ Corresponding authors: Zsafia I Kovacs, PhD, Joseph A Frank, MD, MS, Frank Laboratory, Building 10 Room B1N256, 10 Center Drive MSC 1074, Bethesda, Maryland 20854. Email: zsafia.kovacs@nih.gov, jf5z@nih.gov; Phone: +41 44 633 76 73, +1 301-402-4314

© Ivyspring International Publisher. This is an open access article distributed under the terms of the Creative Commons Attribution (CC BY-NC) license (<https://creativecommons.org/licenses/by-nc/4.0/>). See <http://ivyspring.com/terms> for full terms and conditions.

Received: 2017.12.22; Accepted: 2018.07.26; Published: 2018.09.09

Abstract

Magnetic resonance imaging (MRI)-guided pulsed focused ultrasound (pFUS) combined with microbubbles (MB) contrast agent infusion has been shown to transiently disrupt the blood-brain barrier (BBBD), increasing the delivery of neurotherapeutics to treat central nervous system (CNS) diseases. pFUS interaction with the intravascular MB results in acoustic cavitation forces passing through the neurovascular unit (NVU), inducing BBBD detected on contrast-enhanced MRI. Multiple pFUS+MB exposures in Alzheimer's disease (AD) models are being investigated as a method to clear amyloid plaques by activated microglia or infiltrating immune cells. Since it has been reported that pFUS+MB can induce a sterile inflammatory response (SIR) [1-5] in the rat, the goal of this study was to investigate the potential long-term effects of SIR in the brain following single and six weekly sonications by serial high-resolution MRI and pathology.

Methods: Female Sprague Dawley rats weighing 217 ± 16.6 g prior to sonication received bromo-deoxyuridine (BrdU) to tag proliferating cells in the brain. pFUS was performed at 548 kHz, ultrasound burst 10 ms and initial peak negative pressure of 0.3 MPa (in water) for 120 s coupled with a slow infusion of ~ 460 $\mu\text{L}/\text{kg}$ ($5\text{-}8 \times 10^7$ MB) that started 30 s before and 30 s during sonication. Nine 2 mm focal regions in the left cortex and four regions over the right hippocampus were treated with pFUS+MB. Serial high-resolution brain MRIs at 3 T and 9.4 T were obtained following a single or during the course of six weekly pFUS+MB resulting in BBBD in the left cortex and the right hippocampus. Animals were monitored over 7 to 13 weeks and imaging results were compared to histology.

Results: Fewer than half of the rats receiving a single pFUS+MB exposure displayed hypointense voxels on T2*-weighted (w) MRI at week 7 or 13 in the cortex or hippocampus without differences compared to the contralateral side on histograms of T2* maps. Single sonicated rats had evidence of limited microglia activation on pathology compared to the contralateral hemisphere. Six weekly pFUS+MB treatments resulted in pathological changes on T2*w images with multiple hypointense regions, cortical atrophy, along with 50% of rats having persistent BBBD and astrogliosis by MRI. Pathologic analysis of the multiple sonicated animals demonstrated the presence of metallophagocytic Prussian blue-positive cells in the parenchyma with significantly ($p < 0.05$) increased areas of activated astrocytes and microglia, and high numbers of systemic infiltrating CD68⁺ macrophages along with BrdU⁺ cells compared to contralateral brain. In addition, multiple treatments caused an increase in the number of hyperphosphorylated Tau (pTau)-positive neurons containing neurofibrillary tangles (NFT) in the sonicated cortex but not in the hippocampus when compared to contralateral brain, which was confirmed by Western blot (WB) ($p < 0.04$).

Conclusions: The repeated SIR following multiple pFUS+MB treatments could contribute to changes on MR imaging including persistent BBBD, cortical atrophy, and hypointense voxels on T2w and T2*w images consistent with pathological injury. Moreover, areas of astrogliosis, activated microglia, along with higher numbers of CD68⁺ infiltrating macrophages and BrdU⁺ cells were detected in multiple sonicated areas of the cortex and hippocampus. Elevations in pTau and NFT were detected in neurons of the multiple sonicated cortex. Minimal changes on MRI and histology were observed in single pFUS+MB-treated rats at 7 and 13 weeks post sonication. In comparison, animals that received 6 weekly sonications demonstrated evidence on MRI and histology of vascular damage, inflammation and neurodegeneration associated with the NVU commonly observed in trauma. Further investigation is recommended of the long-term effects of multiple pFUS+MB in clinical trials.

Key words: pulsed focused ultrasound, microbubbles, sterile inflammation, blood-brain barrier, hyperphosphorylated Tau

Introduction

The blood brain barrier (BBB) is composed of endothelial cells, astrocyte endfeet and pericytes held together by tight junction proteins and adherence junction proteins within the neurovascular unit (NVU) [1, 3, 6]. The BBB maintains homeostasis and various approaches have been developed to safely and effectively open or bypass it [7-16]. Image-guided low intensity pulsed focused ultrasound (pFUS) coupled with an infusion of ultrasound (US) contrast agent microbubbles (MB) serves as a noninvasive approach for transiently opening the BBB that can specifically target areas within the brain [17]. Gadolinium (Gd) contrast agent-enhanced magnetic resonance imaging (MRI) can be used to visualize the post-sonication BBB disruption (BBBD), which can be confirmed on histology by extravasation of plasma proteins into the parenchyma [2]. Pulsed FUS+MB can generate acoustic radiation and cavitation forces within targeted tissues. Forces from stable MB oscillations within the vasculature and/or inertial cavitation (unstable oscillations) at the endothelial surface send pressure and/or shock waves into the NVU [18] that can induce a sterile inflammatory response (SIR) [2]. The SIR develops as an immediate cascade of pro-inflammatory and anti-inflammatory cytokines chemokines and trophic factors (CCTF) and damage-associated molecular patterns (DAMPs) associated with BBBD along with immune cell infiltration within the targeted tissues. The SIR also involves cyclooxygenase 2 (COX2) and nuclear factor kappa-light-chain-enhancer of activated B cells (NFκB) pathways [2, 5].

Elevation in heat shock protein 70 (HSP70), a DAMP, has also been detected in pFUS+MB-treated brain and is often part of the complex molecular changes in the parenchyma associated with SIR [19]. However, the upregulation of genes associated with NFκB pathways, which induce SIR, was not observed with the infusion of 10 μL/kg Definity® and pFUS with passive cavitation detection (PCD) feedback six

hours post treatment [4, 5]. These results suggested that pFUS+10 μL/kg Definity®-induced BBBD did not lead to elevations in genes associated with SIR; however, the lack of sampling of tissues at multiple or earlier time points does not preclude that existing baseline levels of cellular mRNA could have resulted in proteomic changes in the targeted tissues [20].

Recently, single or multiple MRI-guided pFUS+MB BBBD were used as a part of proof-of-concept studies for decreasing amyloid β (Aβ) plaque burden or hyperphosphorylated Tau (pTau) with improvement in functional outcomes in models of Alzheimer's disease (AD) [7, 21-26]. AD is associated with chronic inflammation characterized by the accumulation of Aβ aggregates in the extracellular space and intracellular hyperphosphorylated Tau (pTau) within neurons and astrocytes along with microglial activation [24, 27]. Pro-inflammatory cytokines, including tumor necrosis factor alpha (TNFα), interleukin (IL) 1β and IL6, that increase NFκB expression, have been shown to modulate the chronic inflammation in AD [27-30]. Various approaches are under investigation to interrupt the neurodegenerative processes that lead to neuronal death that has been associated with significant morbidity and mortality in AD patients [29, 31-35]. pFUS+MB-induced BBBD coupled with an infusion of specific antibodies reduced Aβ plaques and pTau pathological burden [22, 25, 26, 36]. Clearing of Aβ plaques has also been demonstrated with pFUS+MB-mediated BBBD alone based on the hypothesis that endogenous antibodies enter into the targeted parenchyma, facilitating phagocytosis by activated microglia [7, 23, 37, 38]. Multiple weekly sonications with MB infusions in AD models have focused on the histological changes in the brain and have not routinely included serial follow-up MRIs, which would be used in clinical trials, to evaluate pathological corroboration of the persistence of BBBD, microhemorrhages, or neuronal loss [7, 21, 22, 26, 36, 38].

Here, we report serial brain MRIs following a single or six weekly pFUS+MB resulting in BBBB in the left cortex and the right hippocampus in normal rat. Animals receiving one pFUS+MB treatment had limited MRI and pathological findings at 7 and 13 weeks post sonication. Animals that received 6 weekly pFUS+MB exposures had pronounced changes on MRI, primarily on T2*w images, and on pathological examination when compared to contralateral brain, consistent with damage to the parenchyma.

Methods

Animals and BrdU labeling of endogenous stem cells

The studies were approved by the animal care and use committee at our institution and experiments were performed according to the National Research Council's Guide for the Care and Use of Laboratory Animals (2011) [39]. 6 to 8-week-old female Sprague Dawley® rats were used in all experiments (Charles River Laboratory, Wilmington, MA). Rats first underwent baseline T2-weighted (w) MRI (**Figure 1A**) to exclude brain abnormalities that would serve as exclusion criteria [40]. Rats were then divided into three cohorts (n=6/group) and were sonicated once and euthanized at week (W) 7 or 13 (Group A and B respectively) or were sonicated 6 times weekly and were euthanized at W7 (Group C). In order to determine if pFUS stimulated neurogenesis, rats were treated for three consecutive days with intraperitoneal injections of 5-Bromo-2'-deoxy-uridine (BrdU, 300 mg/kg; B9285, Sigma Aldrich, St. Louis, MO) prior to pFUS+MB to label proliferating cells including neural stem cells *in vivo*. The dose of BrdU was chosen based on a previous report for assaying neurogenesis in rodents [41].

MRI-guided pulsed focused ultrasound and microbubbles

MRI was performed on a 3 T MR scanner (Achieva, Philips Healthcare, Andover, MA) equipped with a surface coil (RK-100, FUS Instruments, Toronto, ON), while anesthesia was ensured by isoflurane (1-3.5%) in 100% O₂ via a nose cone. Throughout MR scans, warm water was circulated under the animals to ensure 37 °C body temperature; a steady respiratory rate was monitored using a pressure sensor (SA Instruments Inc., Stony Brook, NY) and maintained at 40-50 breaths per minute by controlling the level of isoflurane/oxygen mixture. For the pFUS experiment, targeting coordinates were obtained from axial T2w images before sonication: turbo spin echo (TSE) with

repetition time/echo time (TR/TE) of 2000/60 ms. Pulsed FUS was performed with the following parameters: 0.3 MPa or 0.5 MPa peak negative pressure (PNP) measured in water that was applied with a 10 ms burst length and <1% duty cycle with a pulse repetition frequency (PRF) of ~0.5-0.6 Hz (i.e., 120 s/9 focal points in the left frontal cortex including the striatum, 120 s/4 target points in the right hippocampus (**Figure 1B**)) using a single-element spherical FUS transducer (center frequency: 548 kHz, focal number: 0.8, active diameter: 7.5 cm; FUS Instruments, Toronto, ON). pFUS PNP of 0.3 or 0.5 MPa (in water) was selected based on contrast enhancement on GdT1w images depending on animal's age. The center of the FUS transducer was fitted with a hydrophone (822 kHz) for PCD from each focal spot. For this study, PCD data was collected for the sonications and processed using proprietary software from the manufacturer (FUS Instruments, Toronto, ON) and MATLAB (Mathworks, Inc, Natick, MA). PCD data was not used as part of a feedback loop to modulate PNP during sonication because it appeared that the proprietary manufacturer software assumed an infusion of MB at the start of sonication in order to modify PNP as part of the feedback process. In this study, pFUS was not initiated until MB were at near steady-state levels in the vasculature (**Figure 1C**) and the algorithm used for PCD feedback may not be compatible with this infusion protocol [2, 42]. Rats were first infused with 100 µL gadopentetate dimeglumine (Gd, Magnevist, Bayer Healthcare Pharmaceuticals, Inc., MA) via tail vein prior to sonication. Thirty seconds prior to initiating pFUS, an intravenous infusion of Optison™ (GE Healthcare, Little Chalfont, Buckinghamshire, UK, 1.66 µL/s) was started that continued to 100 µL (i.e., 30 s) during sonication to targeted regions in the left cortex anterior to the lateral ventricle and the right hippocampus with nonoverlapping 2-mm diameter focal regions (**Figure 1B-C**). Only one dose of 100 µL Optison™ [5-8×10⁷ MB] was administered as a slow infusion independent of animal weight for all pFUS treatments, which resulted in contrast enhancement consistent with BBBB on GdT1w MRI. The initial dose (Day 0) for all groups was ~460 µL/kg of Optison™ IV. Infusion of MB was separated by >5 min between sonicated regions. Immediately post pFUS+MB, axial T1w images were obtained by TSE (TR/TE 350/12 ms). Groups A and B rats were sonicated once at 0.3 MPa in both locations whereas animals in Group C were sonicated 6 times (**Figure 1A**). Following the third pFUS+MB treatment in the Group C rats, the PNP was increased to 0.5 MPa due to the lack of Gd enhancement on T1w images. Group C rats received progressively lower doses per kg of body weight of

Optison™ as rats became heavier during the study. The subsequent 5 Optison™ doses in Group C rats were as follows: 2nd pFUS=404 µL/kg, 3rd pFUS=442 µL/kg, 4th pFUS=420 µL/kg, 5th pFUS=386 µL/kg, and 6th pFUS=377 µL/kg, which are all equivalent by dose to 5-8×10⁷ MB for each rat. High-resolution MR images at 3 T were obtained with a 7-cm solenoid coil (Philips Research Laboratories, Amsterdam, Netherlands): T2w axial TSE (TR/TE 2769/60 ms), T2*w axial (TR/TE 1301/7.0 ms), number of echoes 5, ΔTE 7.0 ms, flip angle 30°, GdT1w axial TSE (TR/TE 600/20 ms). All high-resolution images at 3 T were interpolated to an image resolution of 100×100 µm in-plane with an acquired slice thickness of 500 µm.

In vivo MRI scans at 9.4 T were performed on a Bruker 9.4 T scanner (Bruker Corp., Billerica, MA) using a Doty radiofrequency quadrature coil (Doty Scientific, Inc., Columbia, SC). 3D T2*w images were then acquired to evaluate the presence of T2* abnormality using multiple gradient echo: TR/TE 60/3.2 ms, ΔTE 60/3.3 ms, number of echoes 14, image resolution 200 µm³ (isotropic). The final T2*w images were generated by combining the multiple echo data with an effective TE of 22.7 ms. Both 3 T and 9.4 T high-resolution MRI scans were obtained at set time-points following pFUS+MB exposures (Figure 1A).

MR image analysis

Quantitative T2* maps of the brain were obtained using MEDx image analysis software (Medical Numerics, Bethesda, MD), fitting the signal intensity (S) of each voxel from the gradient-echo images to a mono-exponential decay as a function of TE: $S_i = S_0 \exp(-TE_i / T2^*)$.

Volume-of-interest (VOI) encompassing each pFUS-treated and contralateral cortex and hippocampal regions over all MRI slices were drawn to extract brain voxels from the T2* maps by an experienced technologist. The total number of voxels from each VOI was determined and used to normalize the frequency distribution of the number of voxels with a specific T2* value using standard spreadsheet software. Normalized histograms of the T2* data were used for further statistical analysis within the range of T2* values from 4 to 98 ms. Lateral ventricular volumes were determined using MEDx image analysis software (Medical Numerics, Bethesda, MD) based on maximizing the contrast between cerebral spinal fluid and parenchyma from the T2w images. The total lateral ventricle volume from each slice was added together for each animal in a group.

Histological staining

Rats (n=6 per group) were euthanized either at 7 weeks (Group A, C) or 13 weeks (Group B) post pFUS

with 4% (w/v) paraformaldehyde perfusion. Fixed brains were embedded in paraffin and sectioned at 3 or 5 µm. Brain sections were stained with hematoxylin and eosin (H&E) and immunofluorescent staining (IFL). IFL detected neuronal nuclear antigen (NueN), glial fibrillary acidic protein (GFAP), ionized calcium-binding adapter molecule 1 (Iba1), cluster of differentiation 68 (CD68) and phosphorylated Tau from at least 3-6 sections from each animal. Every fluorescent staining was counterstained with 4',6-diamidino-2-phenylindole (DAPI) at a concentration of 1 ng/mL to label cell nuclei. Primary antibodies used for IFL: chicken anti-NeuN 1:500 (ABN91 Millipore Burlington, MA) rabbit anti-GFAP 1:1500 (Ab 7260 Abcam, Cambridge, MA), goat anti-Iba1 1:200 (019-19741 Wako Chemicals USA, Inc., VA), mouse anti-CD68 1:400 (Ab 955 Abcam, Cambridge, MA) and anti-BrdU antibody 1:400 (B8434, Sigma Aldrich, St. Louis, MO) according to the manufacturer's instructions for identifying dividing neural stem cells. Mouse anti-phospho Tau (MN1050 Thermo Fisher Scientific Waltham, MA) was used to label phosphorylated Tau-containing cells for immunohistochemistry that was counterstained with hematoxylin. The secondary antibodies were from Abcam (Cambridge, MA) and were used in 1:1000 dilutions for the following antibodies: goat anti-rabbit antibody (Ab102293, Abcam, Cambridge, MA) for GFAP; donkey anti-goat antibody (Ab150129, Abcam, Cambridge, MA) for Iba1; and the donkey anti-mouse antibody (A21059, Thermo Fisher Scientific Waltham, MA) and MACH 2 mouse HRP-polymer goat anti-mouse-HRP secondary antibody (MHRP520 Biocare Medical Pacheco, CA) for pTau that were used at the manufacturer's provided concentration. PB staining was performed as previously described [43] to determine the presence of metallophagocytic cells in the treated cortex and hippocampus.

Microscopy

Aperio ScanScope CS equipped with a 20x air objective (NA=0.75, Leica Microsystems, Buffalo Grove, IL) was used for microscopy. Three sections from each brain were used for quantitative analysis. High magnification (63x) images were taken with an Olympus fluorescence microscope (BX61 Olympus, Center Valley, PA). A laser scanning confocal microscope (model 710, Carl Zeiss AG, Oberkochen, Germany, www.zeiss.com) using Plan-Apochromat objectives (20x air, NA=0.8) was used for confocal microscopy. Illumination was provided by argon-ion (Lasos, Jena, Germany, www.lasos.com), diode and diode-pumped solid-state lasers (Roithner Lasertechnik, Vienna, Austria, www.roithner-laser.com).

Histological analysis

Histological evaluation of the microscopy sections was performed at 20x magnification for both cortex and hippocampal regions of all animals in each group. For Iba1, fluorescence signal was quantified using Image J (Version 1.5; National Institutes of Health, Bethesda, MD) by setting thresholds from 10 fields-of-view (FOV) in the defined regions in pFUS-treated and contralateral brain from three histological sections and the mean fluorescence signal was calculated per animal. For GFAP, positively stained area was quantified relative to the whole treated region with ImageScope Viewing Software (Leica Biosystems Inc., Lincolnshire, IL). Quantification of the numbers of CD68⁺ macrophages and BrdU⁺ cells in treated and contralateral brain were counted manually from IFL and averaged over all animals in the group.

Western blot for phosphorylated Tau

Protein extracts were isolated from paraffin embedded tissue using Qproteome FFPE Tissue Kit (Qiagen Inc., Valencia, CA). Protein extracts were purified with methanol precipitation to remove denaturing agents prior to quantification. 8 M Urea (Sigma Aldrich, St. Louis, MO) was used to reconstitute protein pellets along with a protease phosphatase inhibitor cocktail (Cell Signaling, Boston, MA). The concentration of isolated protein was determined using BCA Protein Assay Reagent (Pierce, Rockford, IL). 10 µg of protein was separated on a NuPAGE 4-12% Bis-Tris precast gel (Thermo Fisher Scientific, Waltham, MA) and electrophoretically transferred to polyvinylidene difluoride (PVDF) membranes (Millipore, Billerica, MA). Membranes were incubated with the primary antibodies against phosphorylated Tau protein 1:1000 (MN1040, Thermo Fisher Scientific, Waltham, MA) and B actin (BA) 1:5000 (ab8227, Abcam, Cambridge, MA) at 4 °C overnight. Chemiluminescent substrate detection (SuperSignal West Pico PLUS Chemiluminescent Substrate, Thermo Fisher Scientific, Waltham, MA) was used to develop bands. Western blots (WB) were performed in triplicates. Densitometry analysis was done using Image J and the signal intensity corresponding to pTau was normalized to BA signal intensity. Electronic 32-bit scans of WB were used for quantification with the rectangular section tool to highlight each band of interest. A profile plot was created representing the relative density of the contents of each band after the straight-line section tool designated the bottom of each curve. Two independent reviewers who did not have knowledge of which bands were assigned to hippocampus or cortex or groups of animals obtained the signal

intensity and groupings, while statistical analysis was performed by a separate author. The enclosed peaks in each profile plot correspond to the dark bands in the original blot. The ratio of relative density for pTau/BA was calculated and plotted.

Statistical analysis

All values are presented as mean ± standard deviation. Statistical analyses and data presentation were performed with Prism (Version 6, GraphPad Software, Inc., La Jolla, CA). Statistical analysis for the T2* histograms to determine mean T2* values was performed using JMP software (Version 13, SAS Institute, jmp.com). Histograms were smoothed by a running average of 5 over the range of T2* values using standard spreadsheet software. For histograms and ventricle volume, Student's paired *t*-test was used to compare descriptive statistics from sonicated to untreated brain within each group at each time point (i.e., week 2, 7 and 13) to avoid changes due to age of the rats.

For histology, unpaired *t*-test was used for comparison. *p* values < 0.05 were considered significant.

Results

MRI findings following single or multiple pFUS+MB exposures

pFUS+MB was performed with 9 focal points to the left (Lt) cortex and 4 focal points to the right (Rt) hippocampus. The experimental outline for the three groups of rats and the timing of BrdU administration are shown in **Figure 1A**. All animals tolerated pFUS+MB to both regions without complications. There was no significant difference at week 7 in the mean weights for Group A (262.3±26.7 g), Group B (280.8±43.1 g) and Group C (265.3±27.4 g) rats. At the end of the 13th week, Group B rats' mean weight was 315.0±34.0 g. Representative MRI at 3 T and 9.4 T from Group A and B rats are presented in **Figure 2**. For this study, **Figure S1-4** contain the acquired sets of rostral to caudal MR images in order to display the extent of pathology in animals presented in **Figure 2-3**. **Figure 2A** contains MRI sections approximately 4 mm from the superficial cortex from a Group A rat. pFUS+MB parameters were used based on contrast enhancement on GdT1w MRI with qualitatively increased signal intensity in areas of BBBB. T2*w images reveal scattered hypointense voxels in the Lt cortex at W2 and W7 post pFUS+MB. There was no evidence of hypointense voxels in the area of the Rt hippocampus. **Figure 2B-C** are representative post contrast T1w, T2*w and T2w images of two Group B rats at ~7.5 mm from the superficial cortex at various time points.

Figure 2B shows no change detected from baseline MRI over the 13 weeks. In **Figure 2C**, the T2*w image at 9.4 T acquired 1 day after pFUS+MB was unchanged compared to the baseline; however, by W2 the rat developed a focal hypointense region in the Lt cortex that persisted through W13. Fifty percent of Group B rats exhibited the appearance of hypointense voxels in sonicated cortex on the T2*w images between day 1 and week 2 MRI sessions. There were no MRI differences between sonicated hippocampus and contralateral parenchyma. Overall, 33-50% of Group A or B rats had evidence of T2* hypointense voxels primarily in the Lt cortex with rare changes in the Rt hippocampus when compared to contralateral brain. There were also no differences in the mean T2* values for the sonicated brain regions or Lt lateral ventricle dilation in Group A and B rats (**Figure 3C-D, 3F and Table S1**).

MRIs from Group C rats displayed evidence of pathology following the second sonication continuing through W7 scans. Variable amounts of contrast enhancement were observed in these rats on GdT1w images immediately post sonication such that by W4, it was necessary to increase the PNP from 0.3 MPa to 0.5 MPa in order to obtain BBB opening in the cortex or hippocampus (**Figure 3A**). The increase in PNP was needed possibly due to changes in skull thickness and weight gain that resulted in a decrease in MB/kg concentration in the animals or possibly shortening of Optison™ intravascular half-life from repeated exposures in the rat [44]. pFUS PNP at 0.5 MPa

starting at the 4th sonication was the minimum pressure that resulted in BBB opening visible on GdT1w 3 T MRI using the infusion protocol for Optison™ (vide supra) with animals inhaling 100% O₂. **Figure 3B** contains representative MRIs obtained at 3 T from two different locations at W7. Fifty percent of Group C rats had persistent BBB opening on GdT1w images along with hyperintense areas on T2w images at W7. All Group C rats had hypointense voxels on T2*w images in the sonicated regions of the brain (**Figure 3B and Figure S4**). A significant difference ($p=0.012$) was detected in the mean T2* values in the Lt cortex for Group C rats after two sonications (**Figure S5, Table S1**). At W7, the T2* values (mean and skewness) were significantly lower in the multiple sonicated Lt cortex ($p<0.001$, $p=0.009$) and Rt hippocampus ($p=0.044$, $p=0.02$) compared to contralateral brain (**Figure 3E, Table S1**). Quantitative analysis of the Lt and Rt lateral ventricle volumes revealed a significant difference ($p=0.03$) in the Group C rats (**Figure 3F**).

For this study, a feedback algorithm based on PCD to control the FUS pressure [42] was not used; however, ultraharmonic frequencies (i.e., frequency (f) at 1.5 and 2.5 from $f_0=548$ kHz) were collected and analyzed to determine if excessive cavitation occurred that would contribute to parenchymal injury (**Figure S6**). We did observe stable cavitation during sonication in all groups. The ultraharmonic frequency measurements did not detect excessive $1.5f_0$ emissions or persistent $2.5f_0$ emissions during sonication (**Figure S6**).

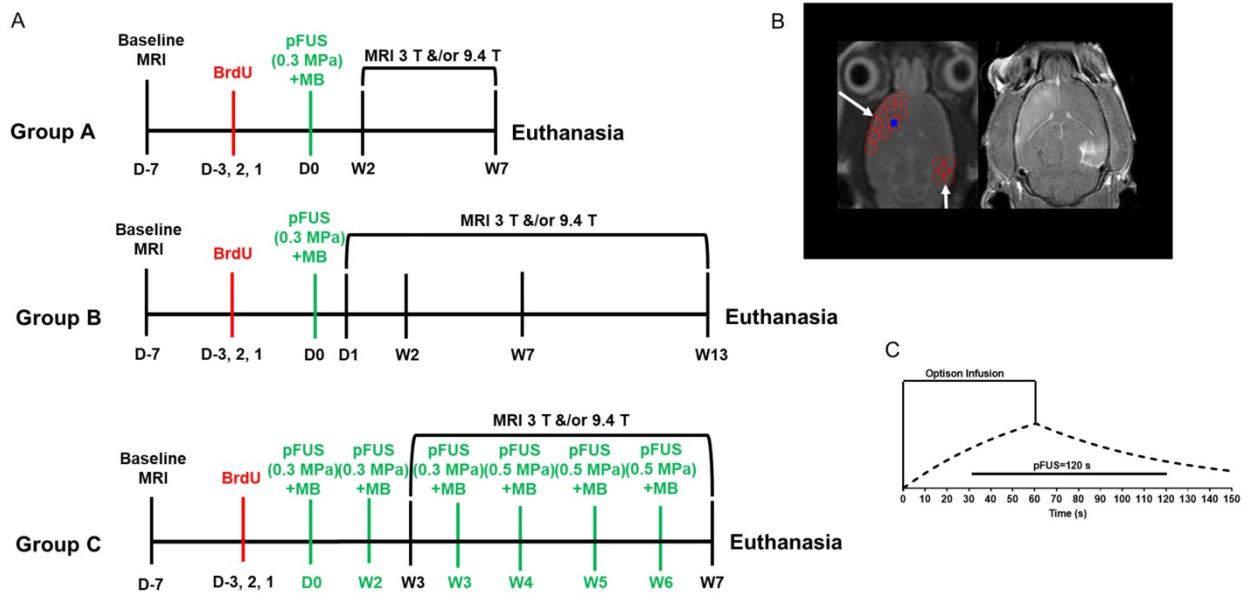


Figure 1. (A) Experimental design. Baseline T2w magnetic resonance images (MRI) were obtained to rule out brain abnormalities prior to sonication. Rats then received a single dose of intraperitoneal 5-bromo-2'-deoxyuridine (BrdU) on three consecutive days before the first pFUS+MB treatment. Axial T2w images were obtained by 3 T MRI for sonication treatment planning: Nine 2 mm-diameter non-overlapping focal points were placed on the left cortex covering the area anterior to the lateral ventricle and 4 focal points were placed on the right hippocampus. Pulsed FUS was coupled with 100 μ L Optison™ MB infusion via the tail vein with 5 min between sonications of the cortex and hippocampus. Post sonication T2w, T2*w and Gd-T1w images were obtained by 3 T MRI, and T2w, T2*w images were obtained by 9.4 T MRI on separate consecutive days. Animals were euthanized and brains were harvested for histological examination at either week (W) 7 or 13. **(B)** GdT1w image at 3 T MRI depicts areas of BBB opening after sonication at PNP=0.3 MPa in the left cortex and right hippocampus. **(C)** Graphic display of the pFUS+MB experimental protocol. 100 μ L Optison™ was infused over 60 s starting 30 s before pFUS at a rate ~ 1.6 μ L/s. The dashed line depicts changes in blood concentration of #MB over time.

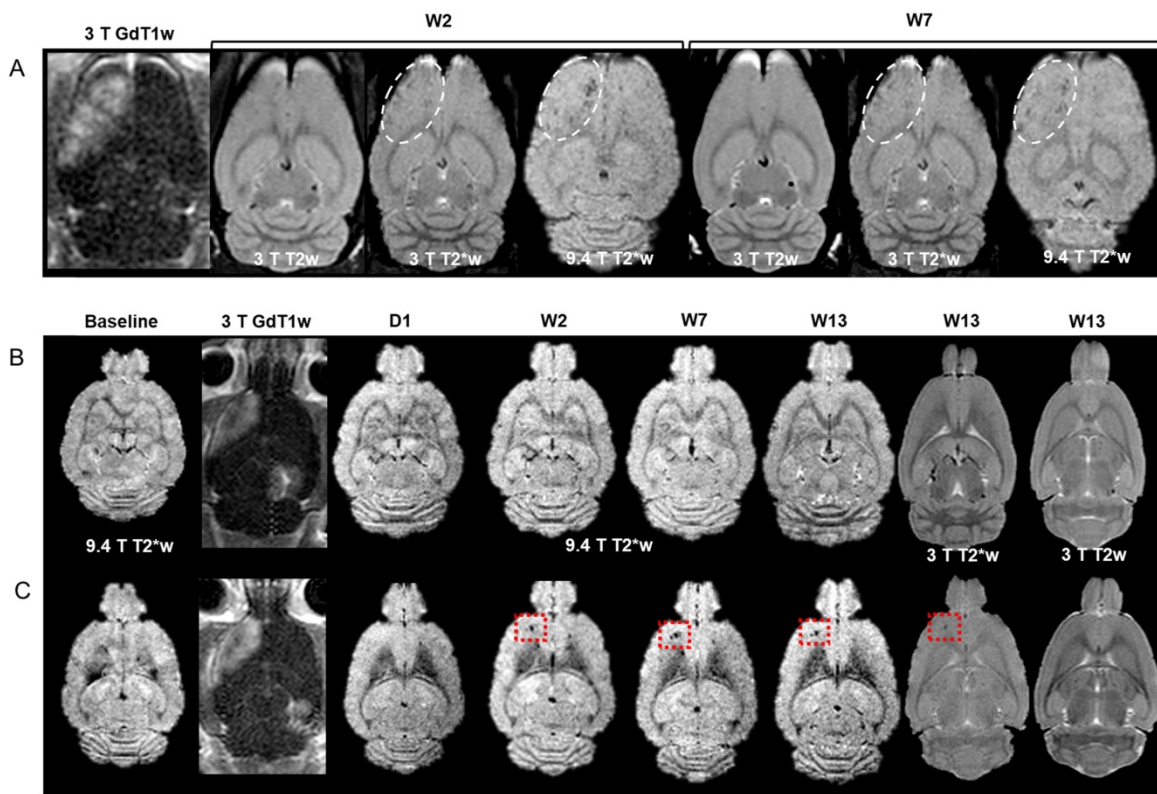


Figure 2. (A) Time course of Gd1w, T2w and T2*w MRI at 3 T, and T2w and T2*w MRI at 9.4 T of a Group A rat brain at ~4 mm from the superficial cortex. Hyperintense regions on T1w images indicate BBBB in the left cortex and right hippocampus. Hypointense regions appear at W2 and W7 post pFUS+MB on 3 T and 9.4 T T2*w images (dashed outline). (B-C) Representative images of two Group B rat brains without (B) and with (C) localized abnormalities in the sonicated left cortex ~7.5 mm from the top of the brain surface. (B) Gd1w images reveal areas of BBBB in the cortex and hippocampus. MRI at any time point did not demonstrate any signal intensity change at either field strength in the targeted parenchyma over the 13 weeks. (C) T2*w images 1 day post pFUS+MB were similar to baseline at 9.4 T. A region of focal hypointensity appeared in the left cortex at W2 that persisted to W13 on 3 T and 9.4 T T2*w images that was not apparent on T2w images at 3 T. There were no observable differences between sonicated hippocampus and contralateral brain. **Figure S1-3** contain rostral to caudal sets of T2*w images at 9.4 T and T2w, T2*w and Gd1w images obtained at 3 T MRI at W7 or W13 for the rats in (A-C) in order to appreciate the extent of MRI changes in each of the rat brains. For all high resolution MR studies, images obtained at 3 T used a slice thickness of 500 μ m and those at 9.4 T used 200 μ m.

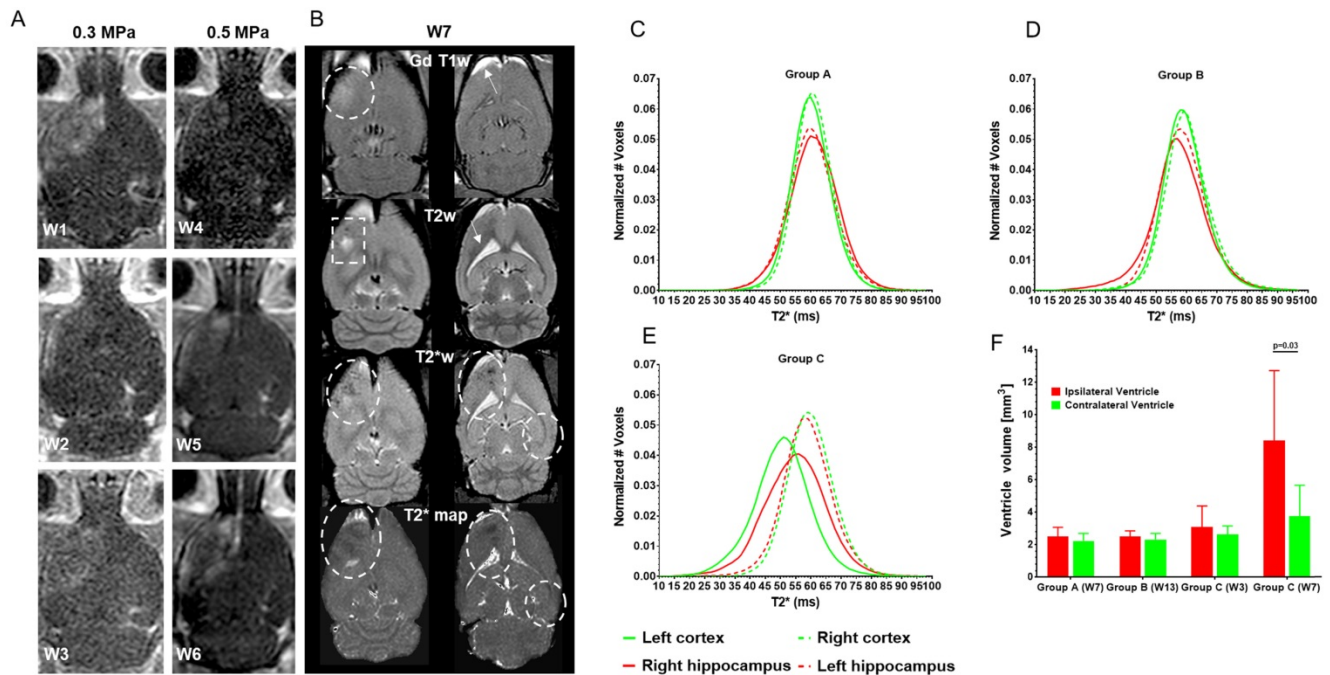


Figure 3. (A-B) Representative MRI from a Group C rat. (A) Gd1w images from the same rat following each of the 6 weekly sonications to the brain. The first three weekly sonications (W1-W3) were performed at PNP=0.3 MPa and the last group of three treatments (W4-W6) at PNP=0.5 MPa. Variable degree of contrast enhancement on Gd1w MRI indicates differences in the degree of BBBB after each sonication. (B) MRI at 3 T at two locations (~4.5 and 7.5 mm from the cortical surface) within the rat brain. Post pFUS+MB images were obtained at one week (W7) following the sixth (i.e., last) treatment. Hyperintense regions in the left cortex on post Gd1w images (dashed lines) demonstrate persistent BBBB at W7 as well as thickening and enhancement of meninges on the ipsilateral side (arrow) with little evidence of contrast enhancement in the right

hippocampal region. T2w images clearly show hyperintense regions in the left cortex (dashed line) consistent with astrogliosis and left lateral ventriculomegaly (arrow) compared to contralateral hemisphere. T2*w images and calculated T2* maps reveal hypointense voxels in both pFUS+MB-treated regions of the brain (dashed circles) consistent with damage, micro-hemorrhages or dilated vessels that were present in all rats receiving 6 weekly sonications. **Figure S4** contains rostral to caudal sets of T2*w images at 9.4 T and T2w, T2*w and GdTIw images obtained at 3 T scanned at W7 for the same rat. **(C-E)** Calculated T2* (ms) histograms derived from T2* maps of all voxels in sonicated and contralateral ventricles (n=6/group). There was no significant difference in mean T2* values between pFUS+MB-treated left (Lt) cortex (green line) and right (Rt) hippocampus (red line) compared to contralateral brain (dashed lines) for Group A and B rats. **(E)** T2* histograms from Group C rats at W7 displaying left shift to significantly lower T2* values for mean and skewness for multiple sonicated Lt cortex ($p<0.001$, $p=0.009$) and Rt hippocampus ($p=0.044$, $p=0.02$) compared to contralateral brain. **Table S1** contains descriptive statistics for mean T2* values, standard deviation, kurtosis and skewness and p values for each of the histograms. **Figure S5** contains T2* histograms for Group C rats following the second weekly pFUS+MB exposure. **(F)** Ventricle volume. Lateral ventricle volume was calculated from 3 T T2w images and demonstrates a significant difference ($p=0.03$) in the ipsilateral Lt ventricle only in Group C rats following 6 weekly pFUS+MB exposures, consistent with cortical atrophy.

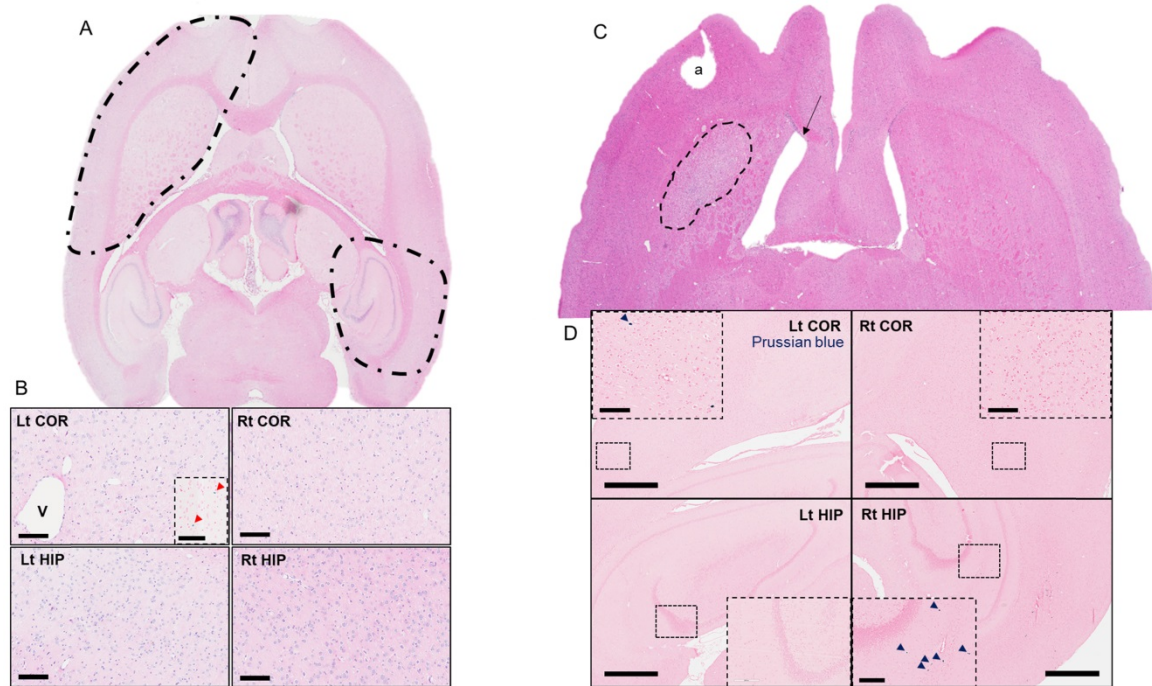


Figure 4. Representative hematoxylin and eosin (H&E) and Prussian Blue (PB) staining of Group B and C rat brains that were obtained at W13 and W7 post pFUS+MB, respectively. **(A)** H&E stain of an axial brain slice representing the two pFUS+MB-treated areas (dashed lines). **(B)** High-magnification H&E images reveal a dilated vessel (V) approximately corresponding to the area of hypointense voxels in **Figure 2C** in a Group B rat that received a single pFUS+MB treatment. Prussian blue staining reveals metallophagocytic PB⁺ cells scattered in the sonicated cortex (Lt COR, insert red arrow) and hippocampus (Rt HIP, not shown) compared to contralateral brain. Scale bar=100 μ m. **(C)** H&E stain of an axial brain slice from the Group C rat in **Figure 3**. The dashed highlighted area represents astrogliosis in the multiple treated cortex approximately corresponding to the hyperintense region in the **Figure 3B** T2w images. The arrow indicates dilated ventricle ipsilateral to the sonicated cortex. **(D)** Prussian blue staining of sonicated and contralateral cortex and hippocampus demonstrates the presence of PB⁺ metallophagocytic cells that are primarily activated systemic macrophages and microglia. These cells contribute to the hypointense voxels observed in treated parts of the brain on T2*w MRI. a: tissue artifact; COR: cortex; HIP: hippocampus. Scale bar=1 mm; insert=100 μ m (COR) and 200 μ m (HIP).

Histological changes following pFUS+MB

Histological evaluations were performed either 7 or 13 weeks after a single or six weekly pFUS+MB exposures. Three 3-5 μ m sections were evaluated (**Figure 4-6** and **Figure S7**) either by bright field or IFL and quantitative analysis was performed based on either area measurements of fluorescent pixels or by count. H&E and PB staining from Group B and C rats revealed the presence of dilated vessels, astrogliotic scar and PB-positive metallophagocytic cells (i.e., microglia or CD68⁺ macrophages) that had phagocytosed red blood cells from microhemorrhages or contained iron metabolites localized in the sonicated regions (**Figure 4**). The presence of PB⁺ cells was observed in animals that had hypointense voxels on T2*w images at 3 T. IFL for activated microglia (Iba1) and astrocytes (GFAP), BrdU to identify neurogenesis, and CD68 for infiltrating systemic macrophages showed differences for the sonicated

regions compared to contralateral brain for the three cohorts (**Figure 5-6** and **Figure S7**). Quantitative analysis (unpaired *t*-test) for the Group A animals (**Figure 7A**) demonstrated that there were relatively small yet significantly different stained areas for GFAP ($p<0.02$) and Iba1 ($p<0.03$) between sonicated and contralateral cortex that were not apparent in Group B rats at W13 (**Figure 7B**). There were also significant increases (Group A: $p<0.02$, Group B: $p<0.05$) in the numbers of BrdU⁺ cells in the treated hippocampi compared to contralateral parenchyma without difference in numbers of cells in the frontal cortices. The numbers of CD68⁺ cells detected were also significantly different in sonicated regions compared to contralateral brain for Group A ($p<0.03$ cortex, $p<0.008$ hippocampus) and B ($p<0.008$ cortex, $p<0.03$ hippocampus) animals (**Figure 7A-B**). In comparison, Group C rats had significantly greater differences in the stained area of GFAP ($p<0.006$,

cortex) and Iba1 ($p < 0.0001$, cortex, hippocampus) in the sonicated brain compared to contralateral brain at W7 (**Figure 7C**). There were also significantly greater numbers of BrdU⁺ ($p < 0.0001$, cortex) and CD68⁺ ($p = 0.0001$, cortex, hippocampus) cells in the treated regions compared to contralateral parenchyma. Quantitative analysis of the IFL sections revealed a greater systemic immune response along with neurogenesis in Group C rats (**Figure 7C**) compared

to the two other groups. For Group A and B rats, the neuroinflammatory and neuro-proliferative processes appeared to dissipate between W7 and W13 (**Figure 7A-B**). However, in Group C rats, the increase in immune response and neurogenesis observed may represent the effects of the last (i.e., 6th) pFUS+MB treatment prior to euthanasia or the cumulative effects from multiple sonications (**Figure 7C**).

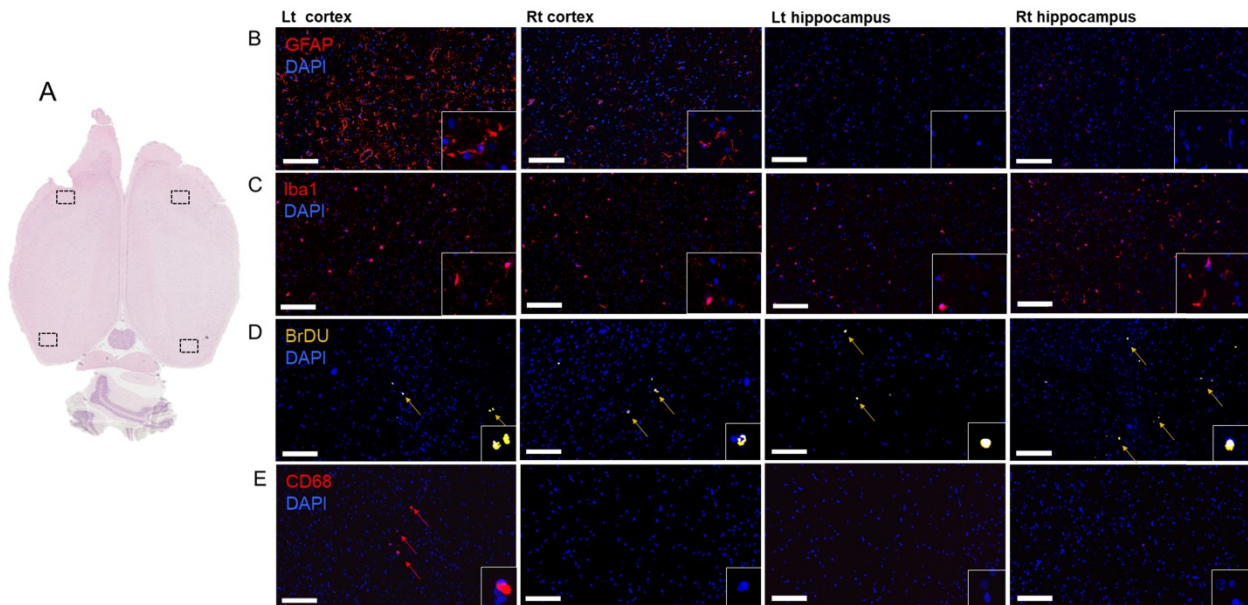


Figure 5. Histological evaluation of the effect of a single pFUS+MB from a Group A rat brain at W7. **(A)** The four boxes on the whole mount H&E image indicate the areas where the representative IFL sections were obtained. **(B)** GFAP and **(C)** Iba1 staining revealed differences between pFUS+MB-treated Lt cortex compared to contralateral brain. **(D)** Evidence of BrdU⁺ cells indicates that neurogenesis was apparent at W7 in the brain and **(E)** CD68⁺ macrophages were observed in the sonicated Lt cortex and Rt hippocampus. Scale bar=100 μm; insert is 63x magnified view of stained cells; 4',6-diamidino-2-phenylindole (DAPI) is the blue nuclear stain.

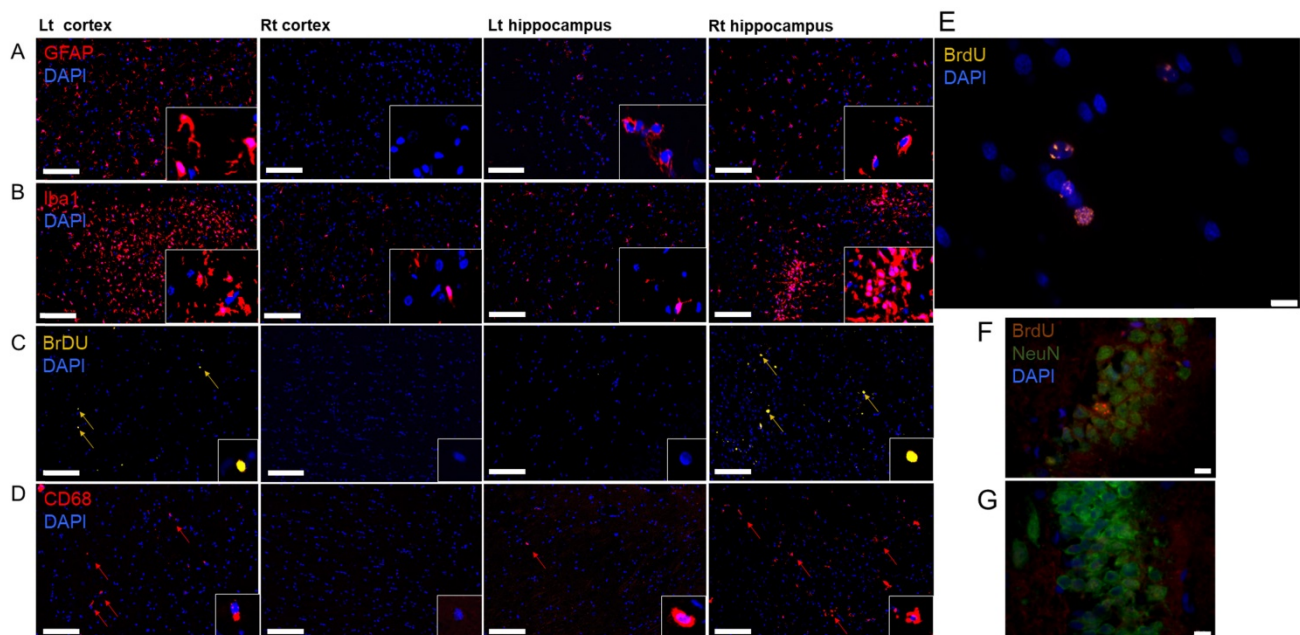


Figure 6. **(A-E)** Immunofluorescent staining of a Group C rat brain following 6 weekly pFUS+MB treatments. **(A)** Increased GFAP expression in the Lt cortex and **(B)** increased Iba1 expression in the Lt cortex and Rt hippocampus consistent with astrocytic and microglia activation in the treated brain regions were observed compared to contralateral brain (Rt cortex and Lt hippocampus). **(C)** BrdU⁺ and **(D)** CD68⁺ cells displayed increased numbers of positive cells in sonicated regions of the brain. Scale bar=100 μm; insert is 63x magnified view of stained cells. **(E)** High-magnification image of BrdU⁺ cells in the treated cortex showed increased BrdU staining colocalized with DAPI (blue nucleus). Scale bar=10 μm. **(F)** Co-localized NeuN⁺ and BrdU⁺ cells from sonicated regions compared to **(G)** contralateral hippocampus. Scale bar=10 μm.

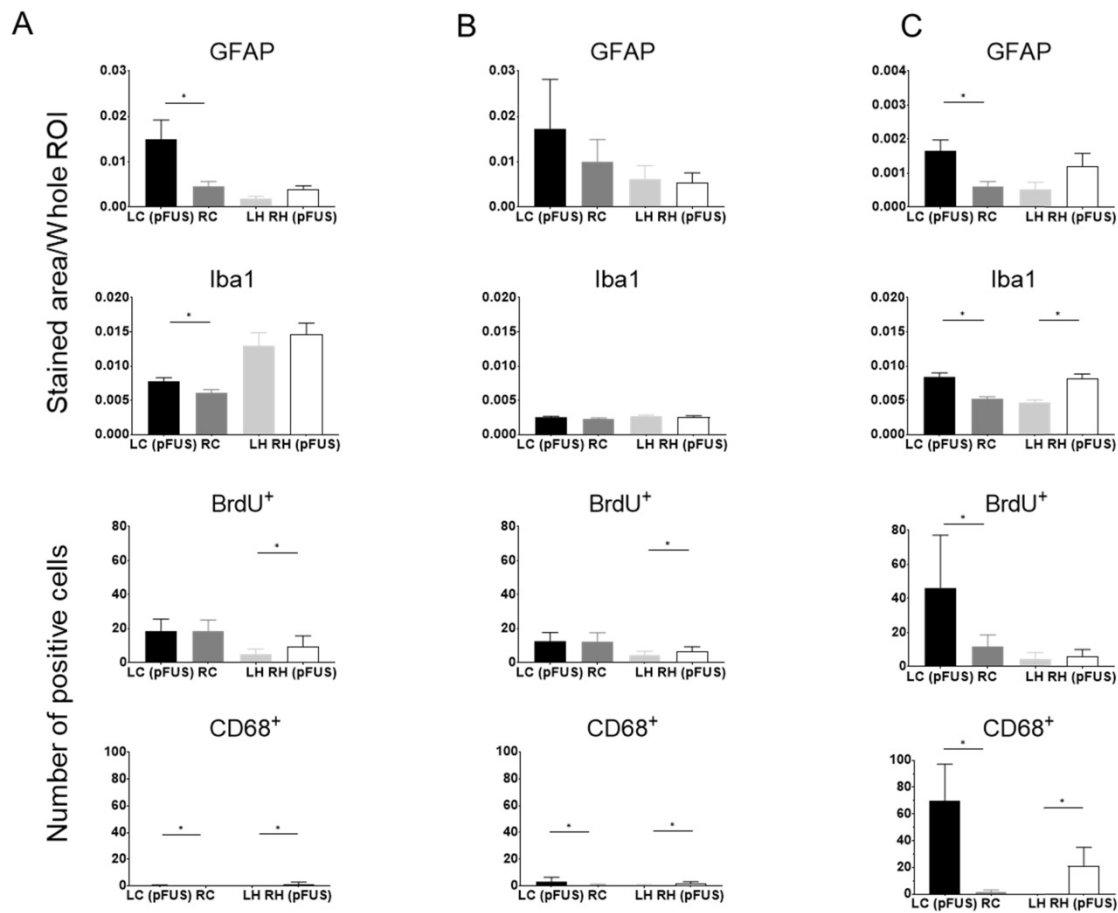


Figure 7. Quantitative analysis of GFAP, Iba1, BrdU⁺ and CD68⁺ staining of sonicated brains at (A) 7 or (B) 13 weeks after a single treatment or (C) 1 week after 6 weekly pFUS+MB treatments. For GFAP and Iba1 staining, the area of positive fluorescence signal was measured using Image J in three consecutive sections ($n=6$ rats/group). Values represent mean stained area/whole region-of-interest (ROI). BrdU⁺ and CD68⁺ cells, co-localized with DAPI, were counted manually in the whole treated area in three consecutive sections from $n=6$ rats per each group. Statistical analyses were based on unpaired *t*-test: LC (pFUS) vs. RC and LH vs. RH (pFUS). Asterisks indicate statistically significant elevations ($p<0.05$). Data are presented as mean \pm SD. LC (pFUS): Lt cortex; RC: Rt cortex; RH (pFUS): Rt hippocampus; LH: Lt hippocampus.

Presence of hyperphosphorylated Tau in the sonicated brain

Multiple courses of pFUS+MB BBBB have been shown to decrease the A β plaques burden in Alzheimer's disease experimental models; however, there has been no report of whether multiple sonications would induce changes in pTau deposition in the brain. **Figure 8** contains representative examples of pTau in neurons on bright-field and by immunofluorescent staining from sonicated cortex (**Figure 8A, 8E**) and to a lesser extent in the hippocampus (**Figure 8D**) in animals that received 6 weekly treatments. Group A and B rats had rare pTau-positive neurons primarily located in the treated cortex but not in the hippocampus. Western blot analysis for pTau (**Figure 8G** and **Figure S8**) revealed significant elevations ($p<0.04$) in sonicated cortex but not in the hippocampus from Group C rats, whereas there were no differences compared to contralateral untreated parenchyma in the animals that received a single pFUS+MB treatment.

Discussion

Several approaches have been developed to effectively open the BBB that include intra-arterial infusion of hypertonic mannitol or bradykinin or experimental pFUS+MB for drug and gene delivery in order to treat neurological diseases [7, 9, 12-14, 45-48]. Image-guided pFUS coupled with intravenous MB serves as a noninvasive approach for opening the BBB that can specifically target areas within the brain [12]. The interaction of the pFUS with MB confined to the vascular space leads to stable cavitation and transient BBBB via stretching of endothelial cells coupled with the induced expression of CCTF from the NVU and alterations in TJP expression [2]. There are several studies investigating the safety of multiple pFUS+MB openings of the BBB in experimental models [45, 49-51] along with clinical trials (clinicaltrials.gov; NCT02986932, NCT03119961, NCT03321487, NCT02343991, NCT03551249). Experimental studies usually do not incorporate advanced high-resolution imaging and histological techniques as part of their

confirmation as to the lack of pathological changes within the targeted brain. Previous reports have correlated MRI findings to limited histological evaluation that includes H&E stains or identification of microglia and astrocytes [21, 45, 50]. A recent safety study in rats that received six weekly pFUS+MB (PNP=0.6-0.8 MPa) at 690 kHz induced BBBB revealed microhemorrhages, macrophage infiltration, cystic cavities and/or dilated small vessels [52]. The

authors stated that repeated sonications in the normal brain were essentially safe with limited or no clinical consequences despite the histological finding. pFUS+MB protocols that include PCD feedback control of PNP during pFUS with an injection of MB should be valuable in order to limit pathological changes in treating regional or global neurodegenerative diseases.

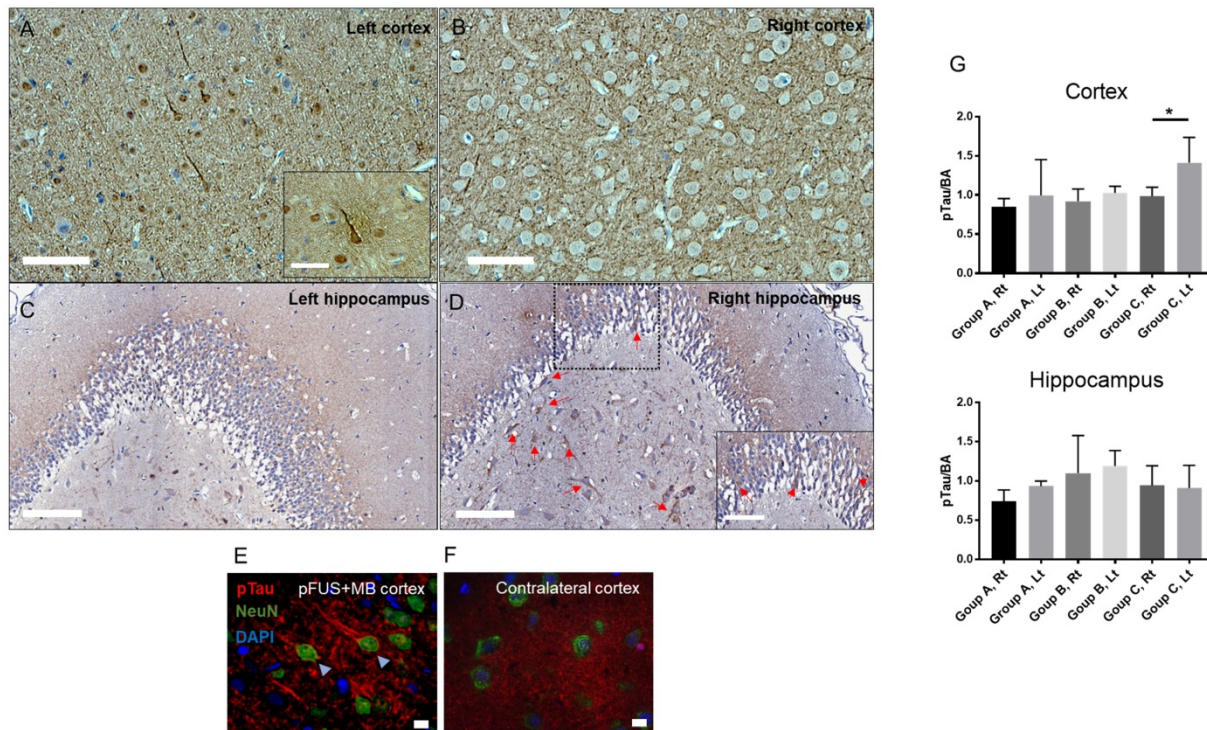


Figure 8. Histological evaluation of hyperphosphorylated Tau (pTau)-positive cells from a Group C rat after 6 weekly pFUS+MB exposures to the brain. Bright field images of the (A) sonicated cortex and (D) hippocampus with neurons (arrows) containing pTau compared to contralateral regions (B-C) of the brain. Scale bars=100 μ m. (E) Triple stained confocal microscopy images of the sonicated cortex show pTau (red) in NeuN⁺ (green) neurons and axons along with the absence of pTau staining in GFAP⁺ astrocytes compared to the contralateral cortex (F). Scale bar for (A-D)=100 μ m and for (E-F)=10 μ m. (G) Quantitative analysis of pTau Western blots (WB) from Lt cortex, Rt cortex, Lt hippocampus, Rt hippocampus and sham control animals normalized to B actin (BA) and plotted as mean \pm SD. Statistical analyses were based on unpaired t-test ($p < 0.04$). **Figure S8** contains examples of WB from sonicated and contralateral brain used for quantitative analyses.

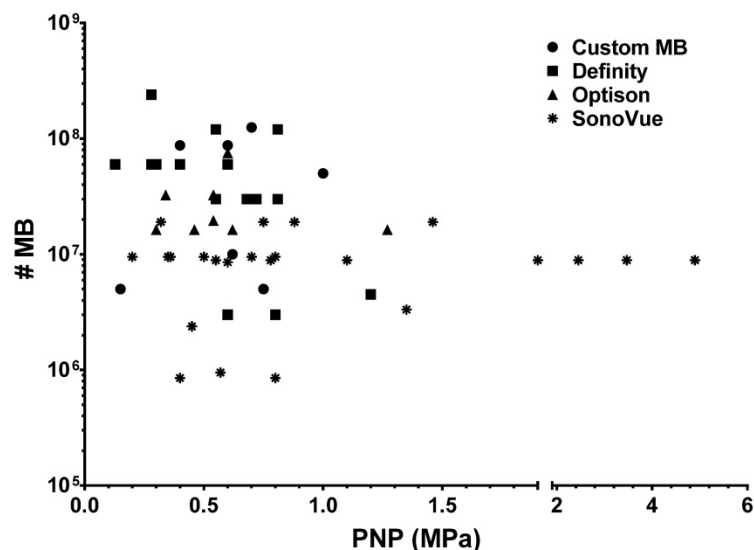


Figure 9. Calculated numbers of MB based on doses provided in **Table S2** for a 250 g rat versus reported peak negative pressure for three clinically approved ultrasound contrast agents and custom MB that have been used to open BBB in rat models.

pFUS+MB BBBD studies continue to require optimization of the FUS parameter feature space (i.e., FUS transducer frequency, PNP, US burst duration, pulse repetition frequency, numbers of focal targets, MB size, dose and infusion rate) in order to adequately deliver agents or cover the canvas of brain pathology to stimulate an endogenous response that may improve functional outcomes [45, 47, 49, 52-54]. Moreover, consistency in the MRI acquisitions (i.e., Gd dose, slice thickness, T1w, T2w and T2*w imaging parameters) across studies is needed to ensure that pathological changes in the targeted brain are not overlooked. Volumetric image analysis should also be included to assess parenchymal loss. In the current study, lower PNP (0.3-0.5 MPa) for the single or multiple weekly pFUS+MB exposures were performed in order to cover large areas of the brain (**Figure 1A-B**), as would be used in treating a large focal region (e.g., ≥ 200 cc) or a diffuse neurological disease.

The pFUS+MB protocol reported here has been shown to induce a SIR with significant elevations in DAMPs (i.e., HSP70, IL1 β) [19], albumin leakage into the parenchyma, and increased release of pro-inflammatory cytokines (i.e., TNF α , interferon gamma) primarily through the NF κ B pathway [2, 5], which have been usually associated with trauma or ischemia [55-59].

To determine if there were prolonged effects of either a single or 6 weekly pFUS+MB in the brain, we monitored pathological changes in the treated parenchyma by MRI followed by histology to understand the long-term effects of the BBBD-associated sterile inflammation. MRI studies performed following a single pFUS+MB BBBD revealed that <50% of the rats had abnormalities on T2*w images. The conspicuity of these hypointense voxels on T2*w images was usually apparent on MRI at 3 T and 9.4 T and would be consistent with either the presence of dilated vessels or iron deposition within phagocytic cells or in the parenchyma. Slow blood flow in dilated vessels could appear as shortened T2* (i.e., hypointensities) due to blood oxygenation-dependent contrast mechanisms that are dependent on the concentration of deoxyhemoglobin in the blood [60]. Animals treated with multiple weekly pFUS+MB exhibited increased numbers of hypointense voxels on T2*w images that initially appeared as early as the second sonication or were visible on week 7 MR scans consistent with parenchymal damage (**Figure 3B, 3E, Figure S4-5**). Moreover, all animals in the Group C cohort demonstrated cortical atrophy associated with dilation of the ipsilateral Lt lateral ventricle consistent with cellular loss (**Figure 3F**). In half of these animals,

the BBB remained open one week following the last sonication (**Figure 3B**). In comparison to other multiple weekly pFUS+MB BBBD studies in the rat in which MRI was used for follow-up and where there were limited pathological changes, the current study clearly showed pathological changes in sonicated regions at 3 T that were confirmed on 9.4 T scans (**Figure 3B**). Our MRI protocols include acquiring voxels with a size of 100 \times 100 μ m in-plane and 500 μ m slice thickness at 3 T in a solenoid receive only coil or 200 μ m³ voxels at 9.4 T with a birdcage coil in order to provide high-resolution scans thereby limiting partial volume effects. In comparison, MRI studies performed at various field strengths (3-7 T) using surface coils and acquired images with 0.8-1.5 mm slice thicknesses and in-plane resolution >200 μ m² following sonication could have under-appreciated or missed pathological changes in the brain because of partial volume effects [2, 47, 61-65]. Future studies should strive to optimize MRI protocols to include higher spatial resolution imaging along with quantitative T1 and T2* maps, and possibly include advanced imaging techniques, such as chemical exchange saturation transfer imaging [66], diffusion basis spectrum imaging [67], or diffusion tensor imaging, [68, 69] to interrogate metabolic, morphological and pathological changes in the brain following multiple pFUS+MB BBBD.

There are differences between the pFUS+MB protocol and histological observations in this study compared to previous reports in which multiple sonications in animal models were performed that need to be addressed. In the current study, the normalized focal area at 548 kHz was 2.5 mm by 17.6 mm at full width half-max calibrated at 1.5 W (equivalent to 1 MPa provided by FUS Instruments, Toronto, ON). pFUS targeting areas were set at 2 mm on center to each other based on our observation on post GdT1w images at 3 T in which the diameter of contrast enhancement was <2 mm and would allow for close placement of focal points in the cortical and hippocampal regions (**Figure 1B**). The goal of this pFUS spacing protocol was to provide as complete coverage of the targeted regions as possible that would be used to deliver agents or stimulate an immune response in the diseased brain. Other reports have used either closely spaced or overlapping foci for pFUS using various sonication parameters coupled with an infusion of MB to open the BBB [4, 47, 61, 63, 64]. Moreover, it has been reported that pFUS with PNP 0.4-0.6 MPa coupled with an infusion of custom MB injected at a dose 3.5 \times 10⁵/g (i.e., 7 \times 10⁷ MB in 200 g rat) did not result in temperature elevations by MR thermometry [70]. Given the sonication parameters of 10 ms US burst and PRF of \sim 0.5 Hz,

which translates into ~ 222 ms between focal spots, therefore, it is unlikely in the current study that temperature elevations contributed to the changes observed on T2*w MRI. In addition, the H&E findings (**Figure 4**) were inconsistent with thermal damage since the histologic changes observed for Group A and B rats when MB was the greatest in this study did not show evidence of necrosis but injury was more consistent with mild vascular injury or trauma.

In this current study, rats were anesthetized with isoflurane anesthesia while inhaling 100% O₂ during pFUS+MB opening of the BBB as compared to other reports in which rats were administered 21% O₂ [4]. Optison™ and Definity® have an intravascular half-life ($T_{1/2}$) of 1.3 min in 21% O₂, which is shortened by $\sim 40\%$ to 0.72 min when animals inhale 100% O₂ [71-73]. MB perfluorocarbon gas is eliminated through the lungs and its clearance rate is governed by first-order principles [20]. Pharmacokinetic modeling would indicate that the infusion rate, initial concentration of injected MB, plasma concentration of MB, $T_{1/2}$, volume of distribution, and oxygenation status all contribute to the numbers of MB exposed to pFUS PNP over the sonication period used to cause BBBD [20]. It has been reported that pFUS+MB BBBD experiments performed while animals inhale 100% O₂ resulted in less enhancement on GdT1w MRI compared to when animals inhaled 21% O₂ [72]. In addition, animals on 100% oxygen had a greater amount of wideband emissions that could have led to an increase in the number of petechia compared to animals breathing air [72], which may appear as hypointense voxels on T2*w MRI. It is important to note that repeated pFUS treatments for opening the BBB with Optison™ and Definity® required 6.5 min ($5 \times T_{1/2} = 390$ s on 21% O₂) in order to avoid the presence of residual intravascular MB in new targeted brain regions [38].

The protocol used in the current study did not incorporate PCD feedback to control the PNP during sonication. pFUS PNP was fixed at either 0.3 MPa on Day 0 for all groups of rats and increased to 0.5 MPa after the 3rd sonication in Group C rats. We changed the pFUS+MB parameters after the 3rd sonication in order to obtain visible BBBD on GdT1w MRI at 3 T. Lower PNPs with the same experimental conditions did not result in reliable or discernible contrast enhancement on GdT1w images. PCD data were not consistent with excessive cavitation doses based on emissions $>3.5 \times$ baseline at $1.5f_0$ and $2.5f_0$ across the multiple focal points (**Figure S6**). Furthermore, broadband signal analyses did not show evidence of inertial cavitation (data not shown). As part of a preliminary study, we performed pFUS with PCD feedback algorithm (FUS Instruments, Toronto, ON)

in combination with the Optison™ infusion protocol (**Figure S9**). There was clear evidence at one focal point starting at the $\sim 30^{\text{th}}$ US burst of the ratio at $0.5f_0$, $1.5f_0$ and $2.5f_0$ being greater than $3.5 \times$ the ratio from the earlier US burst (<30), yet the algorithm did not feedback appropriately on the PNP, allowing pFUS pressures to reach >1 MPa before the appropriate decrease should have occurred. It is possible that the specific PCD feedback algorithm approach [42] was not intended to be used with MB present within the vasculature (**Figure 1C**) along with a subsequent delayed start of pFUS in order to open the BBB. For this reason, PCD feedback was not used in this study. For this reason, PCD feedback was not used in this study.

There is controversy surrounding the protocol consisting of a fixed number of MB (Optison™ dose = $5-8 \times 10^7$ MB or $460 \mu\text{L}/\text{kg}$ to $377 \mu\text{L}/\text{kg}$ over 6 weekly sonications) for Group C rats administered IV prior to the start of sonication as compared to other studies [2, 20, 54, 74]. It has been stated that the Optison™ dose used in this study is 8 to $10 \times$ the clinical imaging dose [2, 19, 52, 73]. The statement assumes that the current study did not abide by a “standardized preclinical protocol” of pFUS+MB to open the BBB. The statement ignores the fact that there is variability in experimental designs in the literature without a discernable standard. Differences in protocols included: the type of MB including coating; MB dispersity; infusion rate; the level of inhaled O₂; initiation of pFUS in relation to MB concentration in the vasculature; as well as the number of foci per region of the brain. Review of the literature would suggest that there is no optimal protocol for the MB dose (independent of US contrast agent being used) and US PNP to cause BBBD. A PubMed search in early 2018 using terms “focused ultrasound, blood brain barrier, safety, and rat” resulted in over 70 published reports with about half providing sufficient information on PNP, type of US contrast agent (SonoVue®, Definity®, Optison™ or custom-made MB), and either $\mu\text{L}/\text{kg}$ or #MB/kg dose used in safely opening the BBB. **Figure 9** is a graph of PNP versus calculated number of MB that would be administered to a 250 g rat to open the BBB based on the available information in **Table S2**. There was no consistent dose or number of MB for the 3 clinically approved US contrast agents and custom MB that have been coupled with pFUS at various frequencies and PNP that result in BBBD (**Table S2**). Most of these reports did not use PCD feedback to determine the possible optimal PNP for BBBD. When evaluating the utility of pFUS+MB to clear A β plaques from the AD mice brains, it is also apparent that a wide range of sonication parameters and MB concentrations has

been used. In one study, pFUS (PNP=0.118+/-0.15 MPa) under PCD feedback control was accompanied by an injection of 20 $\mu\text{L}/\text{kg}$ Definity[®] [7]. Multiple weekly pFUS (PNP 0.3 MPa) with an injection of 80 $\mu\text{L}/\text{kg}$ Definity[®] [38] (i.e., 8 \times the clinical imaging dose of 10 $\mu\text{L}/\text{kg}$) was used to open the BBB and allow influx of endogenous antibodies to clear A β plaques, presumably by inducing an inflammatory response [20, 74]. Another study used scanning ultrasound (SUS) at PNP=0.7 MPa without PCD feedback with a bolus of custom-designed MB at a dose of 4 mL/kg (i.e., 1-5 $\times 10^7$ MB/mL or calculated #MB in 25 g mouse=3.5 $\times 10^6$ MB) [23]. Although it is difficult to directly compare pFUS+MB studies between mice and rats, it appears that the pFUS parameters used in the current study, except for the number of focal spots per PRF, are similar to those used to cause BBBD and clear plaques in AD mice. Moreover, in each of these AD mice studies, multiple weekly sonication studies did demonstrate microglial activation in association with pFUS+MB exposure, but neuropathological examinations for changes in pTau or the presence of NFT in the targeted brain were not performed. These results indicate a need to standardize pFUS+MB protocols that may include real-time PCD with ultraharmonic and broad band emission detection feedback schema [75] to potentially minimize parenchymal damage while still allowing sufficient BBBD to deliver neurotherapeutics or stimulate immune responses.

Regarding MB dosing with pFUS, the Food and Drug Administration (FDA) provides dosing guidelines in the product inserts of Optison[™] (http://www3.gehealthcare.com/~media/documents/us-global/products/contrast-media_non-gatekeeper/clinical-product-information/optison/gehealthcare_optison-prescribing-information.pdf), Definity[®] (http://www.definityimaging.com/prescribing_info.html) and SonoVue[®] (Lumason[®], <https://imaging.bracco.com/us-en/products/contrast-enhanced-ultrasound/lumason>) to be used as injections for US imaging. There are no indications for the use of these US contrast agent MB in combination with pFUS to open the BBB in their respective product inserts. The use of MB with pFUS would be considered an off-label use of the US contrast agents. The combination of MB with pFUS to open the BBB would necessarily be part of an institutional review board (IRB)-approved protocol that would define the dosing and infusion rate based on the risk-benefit analysis provided by the medically responsible investigator filed with their appropriate regulatory commission. Infusions of FDA-approved MB for BBBD may need to be performed at levels greater than those recommended for image contrast according to the

goals of the BBBD study (e.g., stimulation of cellular and humoral immune responses to clear amyloid plaques). Of note, it has recently been reported that following a single or multiple injections of Definity[®] or Optison[™], antibodies most likely developed through a T-cell independent mechanism, which resulted in an effectively shorter half-life ($T_{1/2}$) due to clearance from the vasculature by macrophages [44]. Based on this study, it will probably be necessary to adjust MB dose used with pFUS in studies where multiple BBBD are planned for delivery of neurotherapeutics or stimulation of the immune system [44].

The pathological results following a single or 6 weekly pFUS+Optison[™] induced BBBD in this study are consistent with observations on H&E (**Figure 4**) from other reports in which areas of microhemorrhages, astrogliosis and microglial activation were detected [76, 77]. In Groups A and B rats, the differences between sonicated ipsilateral and contralateral brain decreased with time post sonication by GFAP and Iba1 staining and there were fewer BrdU⁺ and CD68⁺ cells in the targeted regions (**Figure 5**, **Figure S7**). For Group C, in which animals were euthanized 1 week after the 6th sonication, there was significantly increased microglia and astrocyte activation along with increased numbers of BrdU⁺ cells and CD68⁺ cells compared to contralateral parenchyma. In these animals, the apparent difference in Iba1 staining in the treated cortex and hippocampal regions (**Figure 6**) may reflect the proliferative response of microglia in the presence of chronic inflammation that is detected in AD models [78, 79]. The enhanced neurogenesis following pFUS+MB infusion may depend on the US parameters used, with the result of increased expression of trophic factors such as brain-derived neurotrophic factor in the targeted brain [2].

MRI-guided pFUS+MB studies are being proposed as a method to facilitate treatment of neurodegenerative diseases. The combination of pFUS or SUS with MB infusion in AD models has facilitated clearance of A β plaques and pTau from the parenchyma [7, 21-26, 36, 38, 76, 80]. Single and multiple courses of pFUS+MB have also resulted in detectible increases in neurogenesis. It has been hypothesized that the enhanced neurogenesis in both wild type and AD mouse models was associated with an increase in trophic factors such as vascular endothelial growth factor, brain-derived neurotrophic factor, stromal-derived factor-1 alpha and erythropoietin [7, 23, 81-87]. It has been reported that pFUS+MB-induced BBBD increases these trophic factors coupled with antiapoptotic signaling [2, 4]. We hypothesize that pFUS-induced stable cavitation of

MB affects the cellular components of the NVU, inducing increased transient expression of CCTF and CAM that results in a SIR, activating microglia along with an innate immune response that contributes to A β plaques clearance [2, 20, 23, 38, 74]. Future long-term investigations will be required for the durability of A β plaque clearance or if a paradoxical rebound effect can occur overtime resulting in an increase in the numbers of A β plaques or other pathology (i.e., NFT) in the regions of previously sonicated brain.

The accumulation of pTau NFT in neurons has been associated with AD, frontal lobe dementia and chronic traumatic encephalopathy (CTE) [88-92]. The combination of pTau NFT and A β plaques has been associated with neurotoxicity in AD [92]. The ability to clear pTau NFT in AD has been limited because of the inability of antibody-based treatments to cross the intact BBB [25]. The combination of SUS+MB caused BBBD in a human Tau transgenic pR5 mouse model and provided the means to increase delivery of antibody fragment RN2N, resulting in decreases in total Tau with improvements in neurobehavioral studies [25]. The RN2N antibody fragment was shown to inhibit glycogen synthase kinase 3 beta (GSK3 β) phosphorylation of Tau in neurons [93] that can result in the overproduction of Tau and the formation of NFT [94]. Previous studies have reported increases in phosphorylated GSK3 β expression in the brain within the first 24 h after sonication [2, 95, 96]. It is possible that multiple pFUS+MB-mediated BBBD would increase phosphorylated GSK3 β expression and drive the formation of pTau in the targeted "normal" parenchyma, as observed in the current study or in other non-tauopathy-associated diseases. However, it is unknown whether multiple weekly pFUS+MB BBBD can result in increases in pTau in clinical trials [24].

The pFUS+MB protocol used in this study was reported to induce a SIR with significant elevations in DAMPs, albumin extravasation into the parenchyma, and increased expression of pro-inflammatory CCTF and CAM primarily through the NF κ B pathway [4, 5]. Frontotemporal dementia patients with a FTDP-17T phenotype have tauopathy that is associated with neuroinflammation, elevations in IL1 β and COX2, microglia activation and infiltrating systemic macrophages in the brain [97]. Interleukin 1 β is elevated in AD patients and overexpression has been shown to reduce A β plaques by activating microglia [28, 30]. Interleukin 1 β also has a detrimental effect by increasing phosphorylated Tau pathology in an AD mouse model [2]. Increases in IL1 β and COX2 protein or gene expression have been observed following pFUS+MB [2].

In the current study, we detected significant increases in pTau in Group C rats confined to sonicated cortex but not the hippocampus (**Figure 8G**, **Figure S8**). It is unclear why Group C rats did not have quantitative elevation in pTau in the sonicated hippocampus, but possible explanations may include skull thickness differences over the two sonicated regions and neuronal loss. Another possibility is that we sonicated using the same PRF (i.e., ~1.8–2 s) 4 focal spots for the hippocampus and the associated decrease in duty cycle between US burst versus 9 for the cortex may have contributed to the lack of findings. In addition, sufficient protein from the sonicated hippocampus, while avoiding cortex covered in the focal area, could be extracted for WB from 3 of 5 Group C animals, which may have contributed to the inability to detect increased pTau by molecular analysis. We propose that the increased presence of pTau in animals receiving 6 weekly sonications would be linked to the repeated BBBD and sterile inflammation contributing to neurodegenerative processes [97].

We did not observe increases in pTau following a single treatment of pFUS+MB and it is possible that clearance of the damaged pTau-containing neurons occurred over time [98, 99]. Single or multiple contusions have been associated with moderated to severe traumatic brain injury that can result in increased pTau with the presence of NFT consistent with CTE [91, 98, 99]. It is also possible that the coupling of repeated high PNP pFUS+MB BBBD that results in vascular injury and parenchymal damage [52] can be developed into a possible noninvasive model of CTE [89, 100].

Limitations

There are some limitations of this study that should be addressed. The number of animals per cohort was limited to six primarily because of the availability of MRI and pFUS that could be performed over 13 weeks. We plan to perform longer follow-up studies in the 6 weekly pFUS+MB-treated animals to determine if our MRI results (i.e., hypointense voxels, BBBD and atrophy) would be altered. It is possible that there would be clearance of the inflammatory response (i.e., activated microglia, CD68⁺ cells) and pTau over time in animals receiving multiple sonications [99]. The cellular inflammatory changes detected at week 7 following multiple sonications may reflect pathological changes due to the last pFUS+MB treatment. Future studies should evaluate MRI and histological changes 1 week after a single pFUS+MB treatment. The effects of repeated pFUS+MB on the glia limitans, meninges, associated vasculature [101, 102], or alterations in lymphatic

drainage [103] will require further investigation. This study should be repeated in experimental AD models with a gyrencephalic brain (i.e., swine or canine) [47, 104, 105] since it is unknown whether the pFUS+MB would induce a similar magnitude of SIR in humans [2, 106] as observed in the lissencephalic rat brain. It is also unknown if the pathology observed in the current study is related to the brain size or reflection of the FUS from the base of the skull [107]. It has been reported that multiple courses of pFUS+MB to the hippocampus or motor cortex either did not alter neurobehavior [49, 51] or was associated with improvements in functional memory [7]. The results reported here do not completely recapitulate MRI findings from other safety studies involving multiple sonications in healthy experimental subjects and in AD models primarily due to the differences in the pFUS+MB, MRI and pathological protocols used along with sonicated volume of parenchyma and the image analysis performed [7, 21, 23, 45, 47, 51, 52, 108-110].

Conclusion

In summary, pFUS+MB BBBD in the cortex and hippocampus was monitored by serial MRI and histology. We observed biological variability across the two cohorts of animals receiving a single pFUS+MB exposure based on MRI and histology. In comparison, 6 weekly pFUS+MB resulted in significant pathology reflected on MRI and histology presumably resulting from repetitively induced sterile inflammation. The SIR associated with multiple pFUS+MB treatments could contribute to clearance of amyloid plaques from AD patients by stimulating the innate cellular immune system as well as resulting in elevations in pTau levels detected in the cortex of the healthy brain, raising concerns about the feasibility of using this approach in clinical trials that will encompass areas of existing neuropathology. Further investigation is recommended to monitor the inflammatory responses in the brain to multiple pFUS+MB exposures to open the BBB by advanced imaging techniques [68, 111] prior to implementing this approach broadly in clinical trials of neurological diseases.

Abbreviations

A β : amyloid β ; BA: beta actin; BBB: blood-brain barrier; BBBD: blood-brain barrier disruption; BrdU: bromo-deoxyuridine; CAM: cell adhesion molecules; CCF: cytokines chemokines and trophic factors; CD68: cluster of differentiation; CNS: central nervous system; COX2: cyclooxygenase 2; CTE: chronic traumatic encephalopathy; DAMP: damage-associated molecular pattern; DAPI: 4',6-diamidino-2-

phenylindole; *f*: frequency; Gd: gadolinium; GFAP: glial fibrillary acidic protein; GSK3 β : glycogen synthase kinase 3 beta; HSP70: heat shock protein 70; H&E: hematoxylin and eosin; Iba1: ionized calcium-binding adapter molecule 1; IFL: immunofluorescent staining; IL: interleukin; Lt: left; MB: microbubbles; NFT: neurofibrillary tangles; NF κ B: nuclear factor kappa-light-chain-enhancer of activated B cells; NVU: neurovascular unit; PB: Prussian blue; PCD: passive cavitation detection; pFUS: pulsed focused ultrasound; PNP: peak negative pressure; PRF: pulse repetition frequency; pTau: hyperphosphorylated Tau; ROI: region-of-interest; Rt: right; SIR: sterile inflammatory response; S: signal intensity; SUS: scanning ultrasound; TE: echo time; TJP: tight junction proteins; TNF α : tumor necrosis factor α ; TR: repetition time; TSE: turbo spin echo; US: ultrasound; VOI: volume-of-interest; W: week; w: weighted; WB: Western blot.

Supplementary Material

Supplementary figures and tables.

<http://www.thno.org/v08p4837s1.pdf>

Acknowledgements

This work was supported by the Intramural Research Programs of the Clinical Center and of the National Institute of Biomedical Imaging and Bioengineering at the National Institutes of Health. Dr. Tsang-Wei Tu was funded by the Department of Defense through the Center for Neuroscience and Regenerative Medicine (Henry M. Jackson Foundation Award #308049-10.01-60855, USU Site No. CNRM-89-3899).

Author Contributions

JAF, ZIK, TW.T conceptualized study and designed experiments. ZIK, TW.T, MS, BKL, FQ, SRB and NJ carried out the experiments, collected data and analyzed the data. ZIK, JAF wrote the paper.

All authors reviewed the manuscript.

Competing Interests

The authors have declared that no competing interest exists.

References

1. Banks WA. From blood-brain barrier to blood-brain interface: new opportunities for CNS drug delivery. *Nat Rev Drug Discov.* 2016; 15: 275-92.
2. Kovacs ZI, Kim S, Jikaria N, Qureshi F, Milo B, Lewis BK, et al. Disrupting the blood-brain barrier by focused ultrasound induces sterile inflammation. *Proc Natl Acad Sci U S A.* 2017; 114: E75-E84.
3. McConnell HL, Kersch CN, Woltjer RL, Neuwelt EA. The translational significance of the neurovascular unit. *J Biol Chem.* 2017; 292: 762-70.
4. McMahon D, Bendayan R, Hynynen K. Acute effects of focused ultrasound-induced increases in blood-brain barrier permeability on rat microvascular transcriptome. *Sci Rep.* 2017; 7: 45657.

5. McMahon D, Hynynen K. Acute inflammatory response following increased blood-brain barrier permeability induced by focused ultrasound is dependent on microbubble dose. *Theranostics*. 2017; 7: 3989-4000.
6. Zhao Z, Nelson AR, Betsholtz C, Zlokovic BV. Establishment and dysfunction of the blood-brain barrier. *Cell*. 2015; 163: 1064-78.
7. Burgess A, Dubey S, Yeung S, Hough O, Eterman N, Aubert I, et al. Alzheimer disease in a mouse model: MR imaging-guided focused ultrasound targeted to the hippocampus opens the blood-brain barrier and improves pathologic abnormalities and behavior. *Radiology*. 2014; 273: 736-45.
8. Chapman CD, Frey WH, 2nd, Craft S, Danielyan L, Hallschmid M, Schioth HB, et al. Intranasal treatment of central nervous system dysfunction in humans. *Pharm Res*. 2013; 30: 2475-84.
9. Gabathuler R. Approaches to transport therapeutic drugs across the blood-brain barrier to treat brain diseases. *Neurobiol Dis*. 2010; 37: 48-57.
10. Gomez D, Martinez JA, Hanson LR, Frey WH, 2nd, Toth CC. Intranasal treatment of neurodegenerative diseases and stroke. *Front Biosci (Schol Ed)*. 2012; 4: 74-89.
11. Gurlek A, Miller MJ, Amin AA, Evans GR, Reece GP, Baldwin BJ, et al. Reconstruction of complex radiation-induced injuries using free-tissue transfer. *J Reconstr Microsurg*. 1998; 14: 337-40.
12. Hynynen K, McDannold N, Vykhodtseva N, Jolesz FA. Noninvasive MR imaging-guided focal opening of the blood-brain barrier in rabbits. *Radiology*. 2001; 220: 640-6.
13. McDannold N, Vykhodtseva N, Hynynen K. Effects of acoustic parameters and ultrasound contrast agent dose on focused-ultrasound induced blood-brain barrier disruption. *Ultrasound Med Biol*. 2008; 34: 930-7.
14. Neuwelt E, Abbott NJ, Abrey L, Banks WA, Blakley B, Davis T, et al. Strategies to advance translational research into brain barriers. *Lancet Neurol*. 2008; 7: 84-96.
15. Stamatovic SM, Keep RF, Andjelkovic AV. Brain endothelial cell-cell junctions: how to "open" the blood brain barrier. *Curr Neuropharmacol*. 2008; 6: 179-92.
16. Suzuki Y, Nagai N, Umemura K. A Review of the mechanisms of blood-brain barrier permeability by tissue-type plasminogen activator treatment for cerebral ischemia. *Front Cell Neurosci*. 2016; 10: 2.
17. Hynynen K, McDannold N, Vykhodtseva N, Jolesz FA. Non-invasive opening of BBB by focused ultrasound. *Acta Neurochir Suppl*. 2003; 86: 555-8.
18. Goertz DE. An overview of the influence of therapeutic ultrasound exposures on the vasculature: high intensity ultrasound and microbubble-mediated bioeffects. *Int J Hyperthermia*. 2015; 31: 134-44.
19. Alonso A, Reinz E, Fatar M, Jenne J, Hennerici MG, Meairs S. Neurons but not glial cells overexpress ubiquitin in the rat brain following focused ultrasound-induced opening of the blood-brain barrier. *Neuroscience*. 2010; 169: 116-24.
20. Kovacs ZI, Burks SR, Frank JA. Focused ultrasound with microbubbles induces sterile inflammatory response proportional to the blood brain barrier opening: Attention to experimental conditions. *Theranostics*. 2018; 8: 2245-8.
21. Alecou T, Giannakou M, Damianou C. Amyloid beta plaque reduction with antibodies crossing the blood-brain barrier, which was opened in 3 sessions of focused ultrasound in a rabbit model. *J Ultrasound Med*. 2017; 36: 2257-70.
22. Burgess A, Aubert I, Hynynen K. Focused ultrasound: crossing barriers to treat Alzheimer's disease. *Ther Deliv*. 2011; 2: 281-6.
23. Leinenga G, Gotz J. Scanning ultrasound removes amyloid-beta and restores memory in an Alzheimer's disease mouse model. *Sci Transl Med*. 2015; 7: 278ra33.
24. Meng Y, Volpini M, Black S, Lozano AM, Hynynen K, Lipsman N. Focused ultrasound as a novel strategy for Alzheimer disease therapeutics. *Ann Neurol*. 2017; 81: 611-7.
25. Nisbet RM, Van der Jeugd A, Leinenga G, Evans HT, Janowicz PW, Gotz J. Combined effects of scanning ultrasound and a tau-specific single chain antibody in a tau transgenic mouse model. *Brain*. 2017; 140: 1220-30.
26. Raymond SB, Treat LH, Dewey JD, McDannold NJ, Hynynen K, Bacskai BJ. Ultrasound enhanced delivery of molecular imaging and therapeutic agents in Alzheimer's disease mouse models. *PLoS One*. 2008; 3: e2175.
27. Querfurth HW, LaFerla FM. Alzheimer's disease. *N Engl J Med*. 2010; 362: 329-44.
28. Akiyama H, Barger S, Barnum S, Bradt B, Bauer J, Cole GM, et al. Inflammation and Alzheimer's disease. *Neurobiol Aging*. 2000; 21: 383-421.
29. Hong JT. NF-kB as a mediator of brain inflammation in AD. *CNS Neurol Disord Drug Targets*. 2017.
30. Rothwell NJ, Luheshi GN. Interleukin 1 in the brain: biology, pathology and therapeutic target. *Trends Neurosci*. 2000; 23: 618-25.
31. Caselli RJ, Beach TG, Knopman DS, Graff-Radford NR. Alzheimer disease: Scientific breakthroughs and translational challenges. *Mayo Clin Proc*. 2017; 92: 978-94.
32. Morgan D. Immunotherapy for Alzheimer's disease. *J Intern Med*. 2011; 269: 54-63.
33. Ruthirakuhan M, Herrmann N, Suridjan I, Abraham EH, Farber I, Lanctot KL. Beyond immunotherapy: new approaches for disease modifying treatments for early Alzheimer's disease. *Expert Opin Pharmacother*. 2016; 17: 2417-29.
34. Shadfar S, Hwang CJ, Lim MS, Choi DY, Hong JT. Involvement of inflammation in Alzheimer's disease pathogenesis and therapeutic potential of anti-inflammatory agents. *Arch Pharm Res*. 2015; 38: 2106-19.
35. Alzheimer's A. 2016 Alzheimer's disease facts and figures. *Alzheimers Dement*. 2016; 12: 459-509.
36. Jordao JF, Ayala-Grosso CA, Markham K, Huang Y, Chopra R, McLaurin J, et al. Antibodies targeted to the brain with image-guided focused ultrasound reduces amyloid-beta plaque load in the TgCRND8 mouse model of Alzheimer's disease. *PLoS One*. 2010; 5: e10549.
37. Burgess A, Eterman N, Aubert I, Hynynen K. Two-photon microscopy for real-time monitoring of focused ultrasound-mediated drug delivery to the brain in a mouse model of Alzheimer's disease. *Proc Spie*. 2013; 8588.
38. Jordao JF, Thevenot E, Markham-Coultes K, Scarelli T, Weng YQ, Xhima K, et al. Amyloid-beta plaque reduction, endogenous antibody delivery and glial activation by brain-targeted, transcranial focused ultrasound. *Exp Neurol*. 2013; 248: 16-29.
39. National Research Council (U.S.). Committee for the update of the guide for the care and use of laboratory animals, 8th ed. Washington, D.C.: Institute for Laboratory Animal Research (U.S.) & National Academies Press (U.S.); 2011.
40. Tu TW, Turtzo LC, Williams RA, Lescher JD, Dean DD, Frank JA. Imaging of spontaneous ventriculomegaly and vascular malformations in Wistar rats: implications for preclinical research. *J Neuropathol Exp Neurol*. 2014; 73: 1152-65.
41. Wojtowicz JM, Kee N. BrdU assay for neurogenesis in rodents. *Nat Protoc*. 2006; 1: 1399-405.
42. O'Reilly MA, Hynynen K. Blood-brain barrier: real-time feedback-controlled focused ultrasound disruption by using an acoustic emissions-based controller. *Radiology*. 2012; 263: 96-106.
43. Anderson SA, Glod J, Arbab AS, Noel M, Ashari P, Fine HA, et al. Noninvasive MR imaging of magnetically labeled stem cells to directly identify neovasculature in a glioma model. *Blood*. 2005; 105: 420-5.
44. Fix SM, Nyankima AG, McSweeney MD, Tsuruta JK, Lai SK, Dayton PA. Accelerated Clearance of Ultrasound Contrast Agents Containing Polyethylene Glycol is Associated with the Generation of Anti-Polyethylene Glycol Antibodies. *Ultrasound Med Biol*. 2018; 44: 1266-80.
45. Horodyckid C, Canney M, Vignot A, Boisgard R, Drier A, Huberfeld G, et al. Safe long-term repeated disruption of the blood-brain barrier using an implantable ultrasound device: a multiparametric study in a primate model. *J Neurosurg*. 2017; 126: 1351-61.
46. Kroll RA, Neuwelt EA. Outwitting the blood-brain barrier for therapeutic purposes: osmotic opening and other means. *Neurosurgery*. 1998; 42: 1083-99; discussion 99-100.
47. O'Reilly MA, Jones RM, Barrett E, Schwab A, Head E, Hynynen K. Investigation of the safety of focused ultrasound-induced blood-brain barrier opening in a natural canine model of aging. *Theranostics*. 2017; 7: 3573-84.
48. Kovacs Z, Werner B, Rassi A, Sass JO, Martin-Fiori E, Bernasconi M. Prolonged survival upon ultrasound-enhanced doxorubicin delivery in two syngenic glioblastoma mouse models. *J Control Release*. 2014; 187: 74-82.
49. Downs ME, Buch A, Karakatsani ME, Konofagou EE, Ferrera VP. Blood-brain barrier opening in behaving non-human primates via focused ultrasound with systemically administered microbubbles. *Sci Rep*. 2015; 5: 15076.
50. Downs ME, Buch A, Sierra C, Karakatsani ME, Teichert T, Chen S, et al. Long-term safety of repeated blood-brain barrier opening via focused ultrasound with microbubbles in non-human primates performing a cognitive task. *PLoS One*. 2015; 10: e0125911.
51. Olumolade OO, Wang S, Samiotaki G, Konofagou EE. Longitudinal motor and behavioral assessment of blood-brain barrier opening with transcranial focused ultrasound. *Ultrasound Med Biol*. 2016; 42: 2270-82.
52. Kobus T, Vykhodtseva N, Pilatou M, Zhang Y, McDannold N. Safety validation of repeated blood-brain barrier disruption using focused ultrasound. *Ultrasound Med Biol*. 2016; 42: 481-92.
53. Kovacs ZI, Burks SR, Frank JA. Reply to Silburt et al.: Concerning sterile inflammation following focused ultrasound and microbubbles in the brain. *Proc Natl Acad Sci U S A*. 2017: PMC5565475.
54. Silburt J, Lipsman N, Aubert I. Disrupting the blood-brain barrier with focused ultrasound: Perspectives on inflammation and regeneration. *Proc Natl Acad Sci U S A*. 2017: PMC5565470.
55. Amantea D, Micieli G, Tassorelli C, Cuartero MI, Ballesteros I, Certo M, et al. Rational modulation of the innate immune system for neuroprotection in ischemic stroke. *Front Neurosci*. 2015; 9: 147.
56. Chen GY, Nunez G. Sterile inflammation: sensing and reacting to damage. *Nat Rev Immunol*. 2010; 10: 826-37.
57. Denes A, Thornton P, Rothwell NJ, Allan SM. Inflammation and brain injury: acute cerebral ischaemia, peripheral and central inflammation. *Brain Behav Immun*. 2010; 24: 708-23.
58. Gadani SP, Walsh JT, Lukens JR, Kipnis J. Dealing with danger in the CNS: The response of the immune system to injury. *Neuron*. 2015; 87: 47-62.
59. Tuttolomondo A, Pecoraro R, Pinto A. Studies of selective TNF inhibitors in the treatment of brain injury from stroke and trauma: a review of the evidence to date. *Drug Des Devel Ther*. 2014; 8: 2221-38.
60. Moonen CT, van Zijl PC, Frank JA, Le Bihan D, Becker ED. Functional magnetic resonance imaging in medicine and physiology. *Science*. 1990; 250: 53-61.
61. Aryal M, Fischer K, Gentile C, Gitto S, Zhang YZ, McDannold N. Effects on p-glycoprotein expression after blood-brain barrier disruption using focused ultrasound and microbubbles. *PLoS One*. 2017; 12: e0166061.
62. Chai WY, Chu PC, Tsai MY, Lin YC, Wang JJ, Wei KC, et al. Magnetic-resonance imaging for kinetic analysis of permeability changes during focused ultrasound-induced blood-brain barrier opening and brain drug delivery. *J Control Release*. 2014; 192: 1-9.

63. McDannold N, Zhang Y, Vykhodtseva N. Nonthermal ablation in the rat brain using focused ultrasound and an ultrasound contrast agent: long-term effects. *J Neurosurg*. 2016; 125: 1539-48.
64. Treat LH, McDannold N, Vykhodtseva N, Zhang YZ, Tam K, Hynynen K. Targeted delivery of doxorubicin to the rat brain at therapeutic levels using MRI-guided focused ultrasound. *Int J Cancer*. 2007; 121: 901-7.
65. Treat LH, McDannold N, Zhang Y, Vykhodtseva N, Hynynen K. Improved anti-tumor effect of liposomal doxorubicin after targeted blood-brain barrier disruption by MRI-guided focused ultrasound in rat glioma. *Ultrasound Med Biol*. 2012; 38: 1716-25.
66. Tu TW, Ibrahim WG, Jikaria N, Munasinghe JP, Witko JA, Hammoud DA, et al. On the detection of cerebral metabolic depression in experimental traumatic brain injury using Chemical Exchange Saturation Transfer (CEST)-weighted MRI. *Sci Rep*. 2018; 8: 669.
67. Wang Y, Wang Q, Haldar JP, Yeh FC, Xie M, Sun P, et al. Quantification of increased cellularity during inflammatory demyelination. *Brain*. 2011; 134: 3590-601.
68. Sun P, Murphy RK, Gamble P, George A, Song SK, Ray WZ. Diffusion assessment of cortical changes, induced by traumatic spinal cord injury. *Brain Sci*. 2017; 7.
69. Tu TW, Williams RA, Lescher JD, Jikaria N, Turtzo LC, Frank JA. Radiological-pathological correlation of diffusion tensor and magnetization transfer imaging in a closed head traumatic brain injury model. *Ann Neurol*. 2016; 79: 907-20.
70. Nance E, Timbie K, Miller GW, Song J, Louttit C, Klibanov AL, et al. Non-invasive delivery of stealth, brain-penetrating nanoparticles across the blood-brain barrier using MRI-guided focused ultrasound. *J Control Release*. 2014; 189: 123-32.
71. Itani M, Mattrey RF. The effect of inhaled gases on ultrasound contrast agent longevity in vivo. *Mol Imaging Biol*. 2012; 14: 40-6.
72. McDannold N, Zhang Y, Vykhodtseva N. The effects of oxygen on ultrasound-induced blood-brain barrier disruption in mice. *Ultrasound Med Biol*. 2017; 43: 469-75.
73. Mullin L, Gessner R, Kwan J, Kaya M, Borden MA, Dayton PA. Effect of anesthesia carrier gas on in vivo circulation times of ultrasound microbubble contrast agents in rats. *Contrast Media Mol Imaging*. 2011; 6: 126-31.
74. McMahan D, Hynynen K. Reply to Kovacs et al.: Concerning acute inflammatory response following focused ultrasound and microbubbles in the brain. *Theranostics*. 2018; 8: 2249-50.
75. Sun T, Zhang Y, Power C, Alexander PM, Sutton JT, Aryal M, et al. Closed-loop control of targeted ultrasound drug delivery across the blood-brain/tumor barriers in a rat glioma model. *Proc Natl Acad Sci U S A*. 2017; 114: E10281-E90.
76. O'Reilly MA, Hough O, Hynynen K. Blood-brain barrier closure time after controlled ultrasound-induced opening is independent of opening volume. *J Ultrasound Med*. 2017; 36: 475-83.
77. Sierra C, Acosta C, Chen C, Wu SY, Karakatsani ME, Bernal M, et al. Lipid microbubbles as a vehicle for targeted drug delivery using focused ultrasound-induced blood-brain barrier opening. *J Cereb Blood Flow Metab*. 2017; 37: 1236-50.
78. Fuger P, Hefendehl JK, Veeraghavalu K, Wendeln AC, Schlosser C, Obermuller U, et al. Microglia turnover with aging and in an Alzheimer's model via long-term in vivo single-cell imaging. *Nat Neurosci*. 2017; 20: 1371-6.
79. Hefendehl JK, Neher JJ, Suhs RB, Kohsaka S, Skodras A, Jucker M. Homeostatic and injury-induced microglia behavior in the aging brain. *Aging Cell*. 2014; 13: 60-9.
80. Yulug B, Hanoglu L, Kilic E. The neuroprotective effect of focused ultrasound: New perspectives on an old tool. *Brain Res Bull*. 2017; 131: 199-206.
81. Cao L, Jiao X, Zuzga DS, Liu Y, Fong DM, Young D, et al. VEGF links hippocampal activity with neurogenesis, learning and memory. *Nat Genet*. 2004; 36: 827-35.
82. Leinenga G, Langton C, Nisbet R, Gotz J. Ultrasound treatment of neurological diseases--current and emerging applications. *Nat Rev Neurol*. 2016; 12: 161-74.
83. Marti HH. Erythropoietin and the hypoxic brain. *J Exp Biol*. 2004; 207: 3233-42.
84. Reher P, Doan N, Bradnock B, Meghji S, Harris M. Effect of ultrasound on the production of IL-8, basic FGF and VEGF. *Cytokine*. 1999; 11: 416-23.
85. Scarcelli T, Jordao JF, O'Reilly MA, Ellens N, Hynynen K, Aubert I. Stimulation of hippocampal neurogenesis by transcranial focused ultrasound and microbubbles in adult mice. *Brain Stimul*. 2014; 7: 304-7.
86. Stumm RK, Rummel J, Junker V, Culmsee C, Pfeiffer M, Kriegelstein J, et al. A dual role for the SDF-1/CXCR4 chemokine receptor system in adult brain: isoform-selective regulation of SDF-1 expression modulates CXCR4-dependent neuronal plasticity and cerebral leukocyte recruitment after focal ischemia. *J Neurosci*. 2002; 22: 5865-78.
87. Tufail Y, Matyushov A, Baldwin N, Tauchmann ML, Georges J, Yoshihiro A, et al. Transcranial pulsed ultrasound stimulates intact brain circuits. *Neuron*. 2010; 66: 681-94.
88. Iqbal K, Liu F, Gong CX. Tau and neurodegenerative disease: the story so far. *Nat Rev Neurol*. 2016; 12: 15-27.
89. Mez J, Daneshvar DH, Kiernan PT, Abdolmohammadi B, Alvarez VE, Huber BR, et al. Clinicopathological evaluation of chronic traumatic encephalopathy in players of American football. *JAMA*. 2017; 318: 360-70.
90. Noble W, Hanger DP, Miller CC, Lovestone S. The importance of tau phosphorylation for neurodegenerative diseases. *Front Neurol*. 2013; 4: 83.
91. Turner RC, Lucke-Wold BP, Logsdon AF, Robson MJ, Dashnaw ML, Huang JH, et al. The quest to model chronic traumatic encephalopathy: A multiple model and injury paradigm experience. *Front Neurol*. 2015; 6: 222.
92. Wang Y, Mandelkow E. Tau in physiology and pathology. *Nat Rev Neurosci*. 2016; 17: 5-21.
93. Hernandez F, Lucas JJ, Avila J. GSK3 and tau: two convergence points in Alzheimer's disease. *J Alzheimers Dis*. 2013; 33 Suppl 1: S141-4.
94. Kohler C, Dinekov M, Gotz J. Active glycogen synthase kinase-3 and tau pathology-related tyrosine phosphorylation in pR5 human tau transgenic mice. *Neurobiol Aging*. 2013; 34: 1369-79.
95. Baseri B, Choi JJ, Deffieux T, Samiotaki G, Tung YS, Olumolade O, et al. Activation of signaling pathways following localized delivery of systemically administered neurotrophic factors across the blood-brain barrier using focused ultrasound and microbubbles. *Phys Med Biol*. 2012; 57: N65-81.
96. Jalali S, Huang Y, Dumont DJ, Hynynen K. Focused ultrasound-mediated bbb disruption is associated with an increase in activation of AKT: experimental study in rats. *BMC Neurol*. 2010; 10: 114.
97. Bellucci A, Bugiani O, Ghetti B, Spillantini MG. Presence of reactive microglia and neuroinflammatory mediators in a case of frontotemporal dementia with P301S mutation. *Neurodegener Dis*. 2011; 8: 221-9.
98. Hawkins BE, Krishnamurthy S, Castillo-Carranza DL, Sengupta U, Prough DS, Jackson GR, et al. Rapid accumulation of endogenous tau oligomers in a rat model of traumatic brain injury: possible link between traumatic brain injury and sporadic tauopathies. *J Biol Chem*. 2013; 288: 17042-50.
99. McAteer KM, Corrigan F, Thornton E, Turner RJ, Vink R. Short and long term behavioral and pathological changes in a novel rodent model of repetitive mild traumatic brain injury. *PLoS One*. 2016; 11: e0160220.
100. McKee AC, Cantu RC, Nowinski CJ, Hedley-Whyte ET, Gavett BE, Budson AE, et al. Chronic traumatic encephalopathy in athletes: progressive tauopathy after repetitive head injury. *J Neuropathol Exp Neurol*. 2009; 68: 709-35.
101. Roth TL, Nayak D, Atanasijevic T, Koretsky AP, Latour LL, McGavern DB. Transcranial amelioration of inflammation and cell death after brain injury. *Nature*. 2014; 505: 223-8.
102. Russo MV, McGavern DB. Immune Surveillance of the CNS following infection and injury. *Trends Immunol*. 2015; 36: 637-50.
103. Louveau A, Smirnov I, Keyes TJ, Eccles JD, Rouhani SJ, Peske JD, et al. Structural and functional features of central nervous system lymphatic vessels. *Nature*. 2015; 523: 337-41.
104. Head E, Murphey HL, Dowling AL, McCarty KL, Bethel SR, Nitz JA, et al. A combination cocktail improves spatial attention in a canine model of human aging and Alzheimer's disease. *J Alzheimers Dis*. 2012; 32: 1029-42.
105. Smith DH, Chen XH, Nonaka M, Trojanowski JQ, Lee VM, Saatman KE, et al. Accumulation of amyloid beta and tau and the formation of neurofilament inclusions following diffuse brain injury in the pig. *J Neuropathol Exp Neurol*. 1999; 58: 982-92.
106. Fung LK. A sterile animal model for neuroinflammation? *Sci Transl Med*. 2017; 9: eaa14994.
107. O'Reilly MA, Huang Y, Hynynen K. The impact of standing wave effects on transcranial focused ultrasound disruption of the blood-brain barrier in a rat model. *Phys Med Biol*. 2010; 55: 5251-67.
108. Aryal M, Vykhodtseva N, Zhang YZ, McDannold N. Multiple sessions of liposomal doxorubicin delivery via focused ultrasound mediated blood-brain barrier disruption: a safety study. *J Control Release*. 2015; 204: 60-9.
109. McDannold N, Arvanitis CD, Vykhodtseva N, Livingstone MS. Temporary disruption of the blood-brain barrier by use of ultrasound and microbubbles: safety and efficacy evaluation in rhesus macaques. *Cancer Res*. 2012; 72: 3652-63.
110. Samiotaki G, Konofagou EE. Dependence of the reversibility of focused-ultrasound-induced blood-brain barrier opening on pressure and pulse length in vivo. *IEEE Trans Ultrason Ferroelectr Freq Control*. 2013; 60: 2257-65.
111. Lee DE, Yue X, Ibrahim WG, Lentz MR, Peterson KL, Jagoda EM, et al. Lack of neuroinflammation in the HIV-1 transgenic rat: an [(18)F]-DPA714 PET imaging study. *J Neuroinflammation*. 2015; 12: 171.
112. Wu SK, Chu PC, Chai WY, Kang ST, Tsai CH, Fan CH, et al. Characterization of different microbubbles in assisting focused ultrasound-induced blood-brain barrier opening. *Sci Rep*. 2017; 7: 46689.
113. Song KH, Fan AC, Hinkle JJ, Newman J, Borden MA, Harvey BK. Microbubble gas volume: A unifying dose parameter in blood-brain barrier opening by focused ultrasound. *Theranostics*. 2017; 7: 144-52.
114. Park J, Aryal M, Vykhodtseva N, Zhang YZ, McDannold N. Evaluation of permeability, doxorubicin delivery, and drug retention in a rat brain tumor model after ultrasound-induced blood-tumor barrier disruption. *J Control Release*. 2017; 250: 77-85.
115. Chu PC, Chai WY, Tsai CH, Kang ST, Yeh CK, Liu HL. Focused ultrasound-induced blood-brain barrier opening: Association with mechanical index and cavitation index analyzed by dynamic contrast-enhanced magnetic-resonance imaging. *Sci Rep*. 2016; 6: 33264.
116. Cho H, Lee HY, Han M, Choi JR, Ahn S, Lee T, et al. Localized down-regulation of p-glycoprotein by focused ultrasound and microbubbles induced blood-brain barrier disruption in rat brain. *Sci Rep*. 2016; 6: 31201.
117. Kobus T, Zervantonakis IK, Zhang Y, McDannold NJ. Growth inhibition in a brain metastasis model by antibody delivery using focused ultrasound-mediated blood-brain barrier disruption. *J Control Release*. 2016; 238: 281-8.

118. Mulik RS, Bing C, Ladouceur-Wodzack M, Munaweera I, Chopra R, Corbin IR. Localized delivery of low-density lipoprotein docosahexaenoic acid nanoparticles to the rat brain using focused ultrasound. *Biomaterials*. 2016; 83: 257-68.
119. Mead BP, Mastorakos P, Suk JS, Klivanov AL, Hanes J, Price RJ. Targeted gene transfer to the brain via the delivery of brain-penetrating DNA nanoparticles with focused ultrasound. *J Control Release*. 2016; 223: 109-17.
120. Aslund AKO, Berg S, Hak S, Morch Y, Torp SH, Sandvig A, et al. Nanoparticle delivery to the brain--By focused ultrasound and self-assembled nanoparticle-stabilized microbubbles. *J Control Release*. 2015; 220: 287-94.
121. Su WS, Tsai ML, Huang SL, Liu SH, Yang FY. Controllable permeability of blood-brain barrier and reduced brain injury through low-intensity pulsed ultrasound stimulation. *Oncotarget*. 2015; 6: 42290-9.
122. Chu PC, Liu HL, Lai HY, Lin CY, Tsai HC, Pei YC. Neuromodulation accompanying focused ultrasound-induced blood-brain barrier opening. *Sci Rep*. 2015; 5: 15477.
123. Chen PY, Hsieh HY, Huang CY, Lin CY, Wei KC, Liu HL. Focused ultrasound-induced blood-brain barrier opening to enhance interleukin-12 delivery for brain tumor immunotherapy: a preclinical feasibility study. *J Transl Med*. 2015; 13: 93.
124. Aryal M, Park J, Vykhodtseva N, Zhang YZ, McDannold N. Enhancement in blood-tumor barrier permeability and delivery of liposomal doxorubicin using focused ultrasound and microbubbles: evaluation during tumor progression in a rat glioma model. *Phys Med Biol*. 2015; 60: 2511-27.
125. Wu SK, Yang MT, Kang KH, Liou HC, Lu DH, Fu WM, et al. Targeted delivery of erythropoietin by transcranial focused ultrasound for neuroprotection against ischemia/reperfusion-induced neuronal injury: a long-term and short-term study. *PLoS One*. 2014; 9: e90107.
126. Nhan T, Burgess A, Cho EE, Stefanovic B, Lilge L, Hynynen K. Drug delivery to the brain by focused ultrasound induced blood-brain barrier disruption: quantitative evaluation of enhanced permeability of cerebral vasculature using two-photon microscopy. *J Control Release*. 2013; 172: 274-80.
127. Alkins RD, Brodersen PM, Sodhi RN, Hynynen K. Enhancing drug delivery for boron neutron capture therapy of brain tumors with focused ultrasound. *Neuro-oncology*. 2013; 15: 1225-35.
128. Chu PC, Chai WY, Hsieh HY, Wang JJ, Wey SP, Huang CY, et al. Pharmacodynamic analysis of magnetic resonance imaging-monitored focused ultrasound-induced blood-brain barrier opening for drug delivery to brain tumors. *BioMed Res Int*. 2013; 2013: 627496.
129. Aryal M, Vykhodtseva N, Zhang YZ, Park J, McDannold N. Multiple treatments with liposomal doxorubicin and ultrasound-induced disruption of blood-tumor and blood-brain barriers improve outcomes in a rat glioma model. *J Control Release*. 2013; 169: 103-11.
130. Wei KC, Chu PC, Wang HY, Huang CY, Chen PY, Tsai HC, et al. Focused ultrasound-induced blood-brain barrier opening to enhance temozolomide delivery for glioblastoma treatment: a preclinical study. *PLoS One*. 2013; 8: e58995.
131. Park EJ, Zhang YZ, Vykhodtseva N, McDannold N. Ultrasound-mediated blood-brain/blood-tumor barrier disruption improves outcomes with trastuzumab in a breast cancer brain metastasis model. *J Control Release*. 2012; 163: 277-84.
132. Burgess A, Huang Y, Querbes W, Sah DW, Hynynen K. Focused ultrasound for targeted delivery of siRNA and efficient knockdown of Htt expression. *J Control Release*. 2012; 163: 125-9.
133. Park J, Zhang Y, Vykhodtseva N, Jolesz FA, McDannold NJ. The kinetics of blood brain barrier permeability and targeted doxorubicin delivery into brain induced by focused ultrasound. *J Control Release*. 2012; 162: 134-42.
134. Liu HL, Hua MY, Chen PY, Chu PC, Pan CH, Yang HW, et al. Blood-brain barrier disruption with focused ultrasound enhances delivery of chemotherapeutic drugs for glioblastoma treatment. *Radiology*. 2010; 255: 415-25.
135. Liu HL, Wai YY, Chen WS, Chen JC, Hsu PH, Wu XY, et al. Hemorrhage detection during focused-ultrasound induced blood-brain-barrier opening by using susceptibility-weighted magnetic resonance imaging. *Ultrasound Med Biol*. 2008; 34: 598-606.